AD-A121 309 EFFECTS OF PARTIAL SUPPRESSION OF ION EMISSION IN MODERATE IMPEDANCE DIODES(U) NAVAL RESEARCH LAB WASHINGTON DC R J BARKER ET AL. 30 SEP 82 NRL-MR-4915 1/1

UNCLASSIFIED F/G 12/1 NL

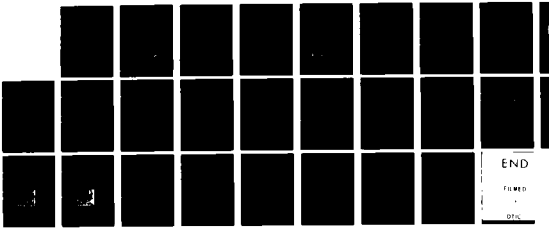

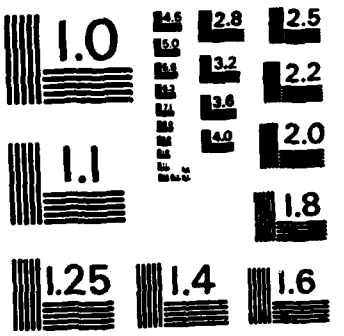

NRL Memorandum Report 4915

(2)

Effects of Partial Suppression of Ion Emission in Moderate Impedance Diodes

ROBERT J. BARKER AND SHYKE A. GOLDSTEIN

JAYCOR, Inc.
Alexandria, VA 22304

September 30, 1982

This research was sponsored in part by the Defense Nuclear Agency under Subtask T99QAXLA014, work unit 46 and work unit title "Ion Beam Generation" and by the Department of Energy, Washington, D.C.

NAVAL RESEARCH LABORATORY
Washington, D.C.

SECURITY CLASSIFICATION OF THIS PAGE (When Data Entered)

REPORT DOCUMENTATION PAGE		READ INSTRUCTIONS BEFORE COMPLETING FORM
1. REPORT NUMBER NRL Memorandum Report 4915	2. GOVT ACCESSION NO.	3. RECIPIENT'S CATALOG NUMBER
4. TITLE (and Subtitle) EFFECTS OF PARTIAL SUPPRESSION OF ION EMISSION IN MODERATE IMPEDANCE DIODES		5. TYPE OF REPORT & PERIOD COVERED Interim report on a continuing NRL problem. 6. PERFORMING ORG. REPORT NUMBER
7. AUTHOR(s) Robert J. Barker* and Shyke A. Goldstein*		8. CONTRACT OR GRANT NUMBER(s)
9. PERFORMING ORGANIZATION NAME AND ADDRESS Naval Research Laboratory Washington, DC 20375		10. PROGRAM ELEMENT, PROJECT, TASK AREA & WORK UNIT NUMBERS 47-0879-0-2 DOE Task No. 14 47-0875-0-2 DNA Subtask No. T99QAXLA, Work Unit 00023
11. CONTROLLING OFFICE NAME AND ADDRESS Department of Energy, Washington, DC 20545 Defense Nuclear Agency, Washington, DC 20305		12. REPORT DATE September 30, 1982 13. NUMBER OF PAGES 34
14. MONITORING AGENCY NAME & ADDRESS(if different from Controlling Office)		15. SECURITY CLASS. (of this report) UNCLASSIFIED 15a. DECLASSIFICATION/DOWNGRADING SCHEDULE

16. DISTRIBUTION STATEMENT (of this Report)

Approved for public release, distribution unlimited.

17. DISTRIBUTION STATEMENT (of the abstract entered in Block 20, if different from Report)

18. SUPPLEMENTARY NOTES

This research was sponsored in part by the Defense Nuclear Agency under Subtask T99QAXLA014, work unit 46 and work unit title "Ion Beam Generation" and by the Department of Energy, Washington, D.C.

*JAYCOR, Inc., Alexandria, VA 22304

19. KEY WORDS (Continue on reverse side if necessary and identify by block number)

Numerical simulation
Intense ion beams
Pinch-reflex diode
Numerical error analysis

20. ABSTRACT (Continue on reverse side if necessary and identify by block number)

Numerical simulations have been completed testing the effects of partial ion emission suppression in 4-5 Ω pulsed power diodes. They were conducted to obtain physical insight into the results of a series of parallel experiments conducted on the Gamble II machine at NRL. A standard axial diode with a 3.0 cm outer radius hollow cathode and an electron reflexing anode foil was found to operate at 1.8 MV and 4.8 Ω with an effective ion efficiency of 0.32. Suppressing ion emission along the anode foil beyond a radius equal to the inner radius of the

(Continued)

DD FORM 1 JAN 73 1473 EDITION OF 1 NOV 65 IS OBSOLETE
S/N 0102-014-6601

SECURITY CLASSIFICATION OF THIS PAGE (When Data Entered)

20. ABSTRACT (Continued)

hollow cathode raised the diode impedance at the same voltage to 6.7 Ω and lowered the effective ion efficiency to 0.29. Decreasing the anode-cathode (A-K) gap from 5.0 mm to 3.5 mm and retaining the same degree of ion emission suppression lowered the impedance again in 4.8 Ω and returned the effective ion efficiency again to 0.32. That efficiency is in good agreement with the experimental findings for the same 3.5-mm gap case but is 0.03-0.07 higher than that experimentally observed for the 5.0-mm gap without ion emission suppression. The discrepancy may be actual or it may be due to a return electron current which masks some of the experimentally observed ion current for that case.

CONTENTS

EFFECTS OF PARTIAL SUPPRESSION OF ION EMISSION IN MODERATE IMPEDANCE DIODES

I. INTRODUCTION

The efficient generation of intense beams of energetic light ions is a central objective of the NRL Light Ion Fusion Research Program.[1] Over the past several years, focused ion current densities of over 100 kA/cm^2 from terrawatt-level beams have been achieved with magnetically insulated radial diodes at Sandia National Laboratories[2] as well as with pinch-reflex axial diodes at the Naval Research Laboratory.[3] Using diodes of below 2 ohm impedance, ion beam efficiencies of over 70% were achieved in both of the above configurations[4,5] (i.e., over 70% of the power coupled to the diodes was carried by the light ions generated therein). The question of ion efficiency is critical to the goal of a practical light ion driven inertial confinement fusion (ICF) reactor. As much as possible of a given pulsed power generator's energy must be imparted to the ion beam exiting the diode in order to minimize the number of beam sources necessary for successful pellet ignition as well as to maximize the overall reactor efficiency. These efficiency considerations are well met by the low impedance diodes.

Unfortunately, the high current densities of the ion beams produced by low impedance diodes are not compatible with the focusing and transport systems presently under study for bringing the beams to bear on the proposed fusion targets.[6] In addition, there are strong arguments in favor of high voltage, the use of high impedance generators in present reactor scenarios.[7] Diodes matched to such generators must likewise be of high impedance to ensure efficient power transmission but such diodes are plagued by relatively low ion production efficiencies. These low efficiencies are a direct consequence of established diode theory. It has been found semiempirically[8] that the total current flowing through a pinched-beam diode may be approximated by

$$I = I_e + I_i \approx 9(\gamma^2 - 1)^{1/2}\frac{R}{D}\left[1 + \left(\frac{eV}{2m_ic^2}\right)^{1/2}\frac{R}{D}\right] \tag{1}$$

where $\gamma = 1 + \frac{V(\text{in } MV)}{0.511}$, R = cathode radius, D = axial anode-cathode (A-K) gap, V = diode voltage, and m_i = ion (proton) mass. Implicit in this formula is an ion-to-electron current ratio given by

$$\frac{I_i}{I_e} \geq 0.5\frac{v_i}{c}\frac{R}{D} \tag{2}$$

where v_i is the mean ion velocity.[9] Thus, for a fixed voltage, increasing the diode impedance translates to decreasing the aspect ratio, R/D. That, in turn, results in a decrease of the current ratio I_i/I_e and a lowering of the ion production efficiency, $I_i/(I_e + I_i)$. This is the crux of the problem addressed by this report. The essence of the proposed solution is an attempt to decouple the impedance from its R/D dependence while exploiting the theorized efficiency enhancement gained through a decreased gap size, D.

For fixed values of R, D, and voltage, the net diode current can be changed from that predicted in Eq. (1) by restricting the emission of electrons from the cathode and ions from the anode respectively.

Manuscript submitted July 23, 1982.

As a starting point, take the standard pinch-reflex diode (PRD) geometry shown in Figure 1. Typical electron and ion trajectories are as sketched. The predominant flow of electrons originates from the cathode shank tip. Electrons emitted there stream to the thin, polyethylene anode foil (pinching radially as they cross the $A-K$ gap if the critical diode current is exceeded[10]). They then pass through the foil with an appropriate loss of energy. Finally they are reflected back through the foil by the large azimuthal magnetic field, B_θ, which is present between the foil and the solid anode surface. This reflection (or "reflexing") process continues as the electrons cascade toward the diode's central axis where they are funneled off through the anode stalk. The hydrocarbon anode plasma formed along the foil meanwhile acts as a rich source of protons which are accelerated in the opposite direction toward the cathode. Proton emission can be expected everywhere the anode plasma has formed including regions along the foil at larger radii than the outer radius of the cathod shank. Ions emitted at radii above the inner radius of the cathode shank are useless for light ion research for two major reasons. First of all, their trajectories differ so little from straight lines that, assuming a planar anode foil, they will probably all hit and be absorbed by the solid cathode shank and thus be unavailable for extraction from the diode. Secondly, their presence near the cathode tip will further increase the emission of electron current with presumably detrimental results to the overall ion production efficiency.

These considerations lead one to conclude that significant benefit could be derived by suppressing the emission of ions from those outer regions of the anode foil face. This is accomplished experimentally by covering the plastic anode foil beyond the inner cathode radius with a thin metal foil (on Gamble II, first tantalum then aluminum was used[11]). This concept has been tested at NRL with very favorable results[12] which will be discussed later. The numerical simulations reported herein modeled the steady-state operation of those experimental diodes. The empirical data showed that suppression of the peripheral ion emission both decoupled the diode impedance from R/D (thus allowing a smaller D for a given impedance) and also significantly enhanced the ion efficiency in comparison to a diode with the same impedance but with larger D and full anode ion emission. The computer runs confirmed the impedance decoupling from R/D but failed to detect any significant ion efficiency enhancement. However, the numerically observed ion efficiency of the diode with ion suppression and small D does agree with the experimental results. Furthermore, the simulation suggests a possible physical mechanism whereby the true magnitude of the net ion current could have been partially masked in the "benchmark" (i.e., full anode ion emission) experiments by a comoving electron current.

II. THE DIODE AND ITS NUMERICAL MODEL

The actual Gamble II experimental diode configuration is drawn in Figure 2. For the discussions presented later in this report, it is particularly important to note the structure of the inner cathode assembly. The "target" is a sheet of KIMFOL stretched over an inner cylindrical cathode shank of radius 2.25 cm. Only the ions flowing within that radius can be extracted from the diode and counted in the experimental $(I_{NET})_{ion}$ measurements. For ease of numerical modeling, the actual diode of Figure 2 was simplified slightly to the form depicted in Figure 3. The anode foil radius was shortened from about 6.0 cm to 3.7 cm. Since that is still almost a centimeter larger than the cathode outer radius the electric field structure along the electron-emitting cathode shank and along the anode's ion-emitting regions opposite the cathode shank should not be significantly modified. In addition, the axially bounding, solid cathode and anode surfaces are taken as completely planar and parallel. The front surface of the cathode "door" (see Figure 2) coplanar with the "target" face. Finally, the thickness of the cathode shank is taken as 0.35 cm while in the experiments it was usually 0.25 cm. The extra millimeter allows for somewhat better numerical resolution over the all-important tip of the shank where most of the net electron current is emitted. Having fixed the essential geometry, it is a straightforward process to implement the numerical model.

NRL's DIODE2D computer code was employed to numerically simulate the steady-state operating conditions for this diode for various sets of parameters. The details of the code may be found elsewhere.[13] It is sufficient here to point out that DIODE2D calculates equilibrium electric and magnetic field strengths over an $NZ \times NR$ mesh of discrete data points on a predetermined computational region

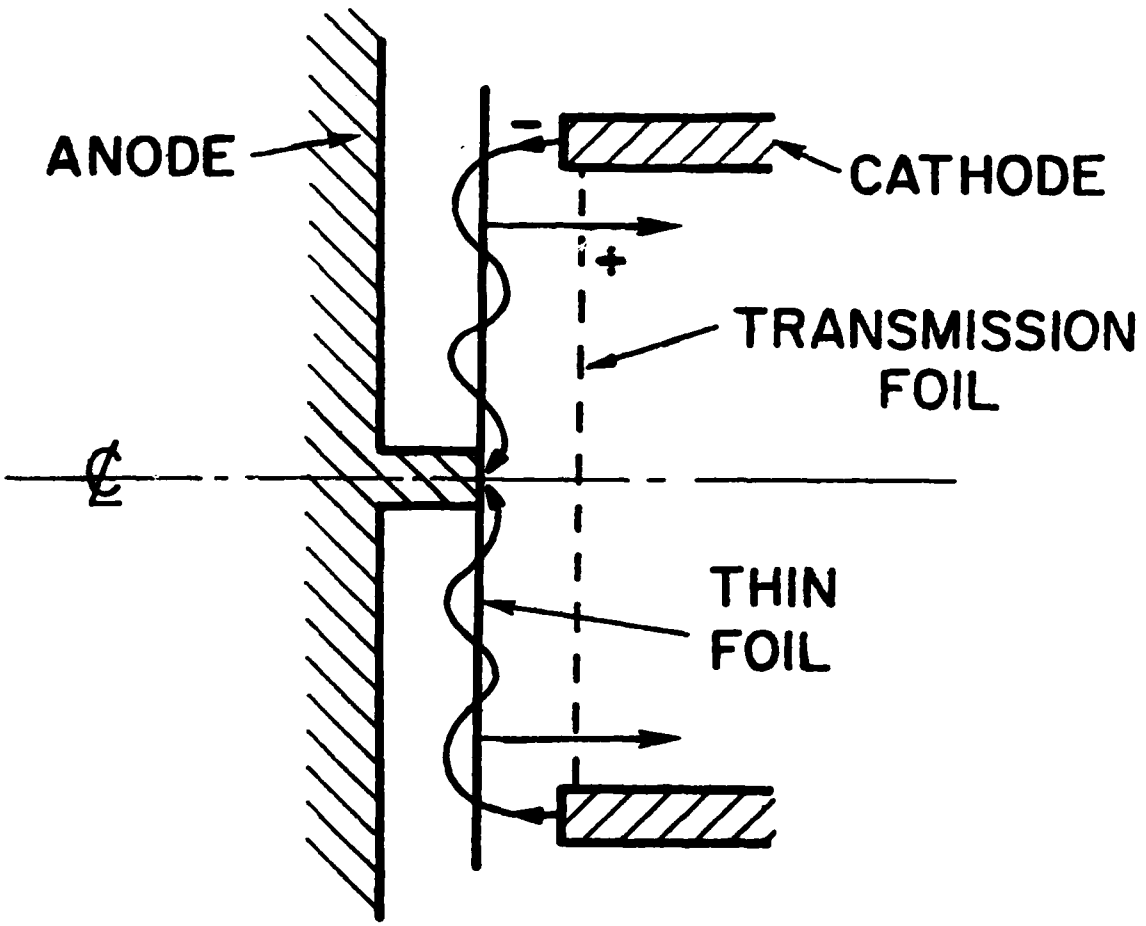

Fig. 1 — The pinch-reflex diode

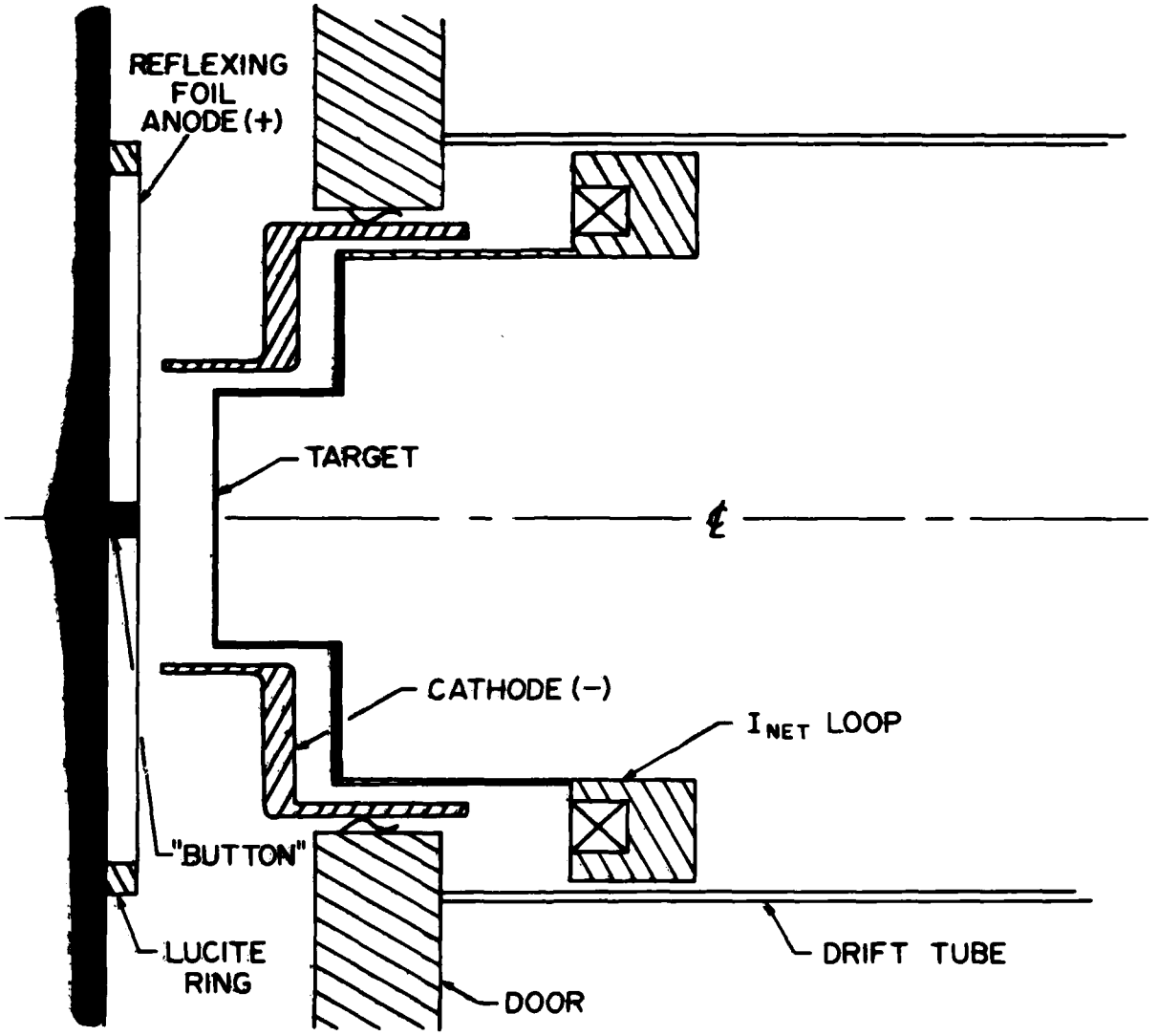

Fig. 2 — The high impedance Gamble II test diode for PBFA-I
(courtesy of S. J. Stephanakis)

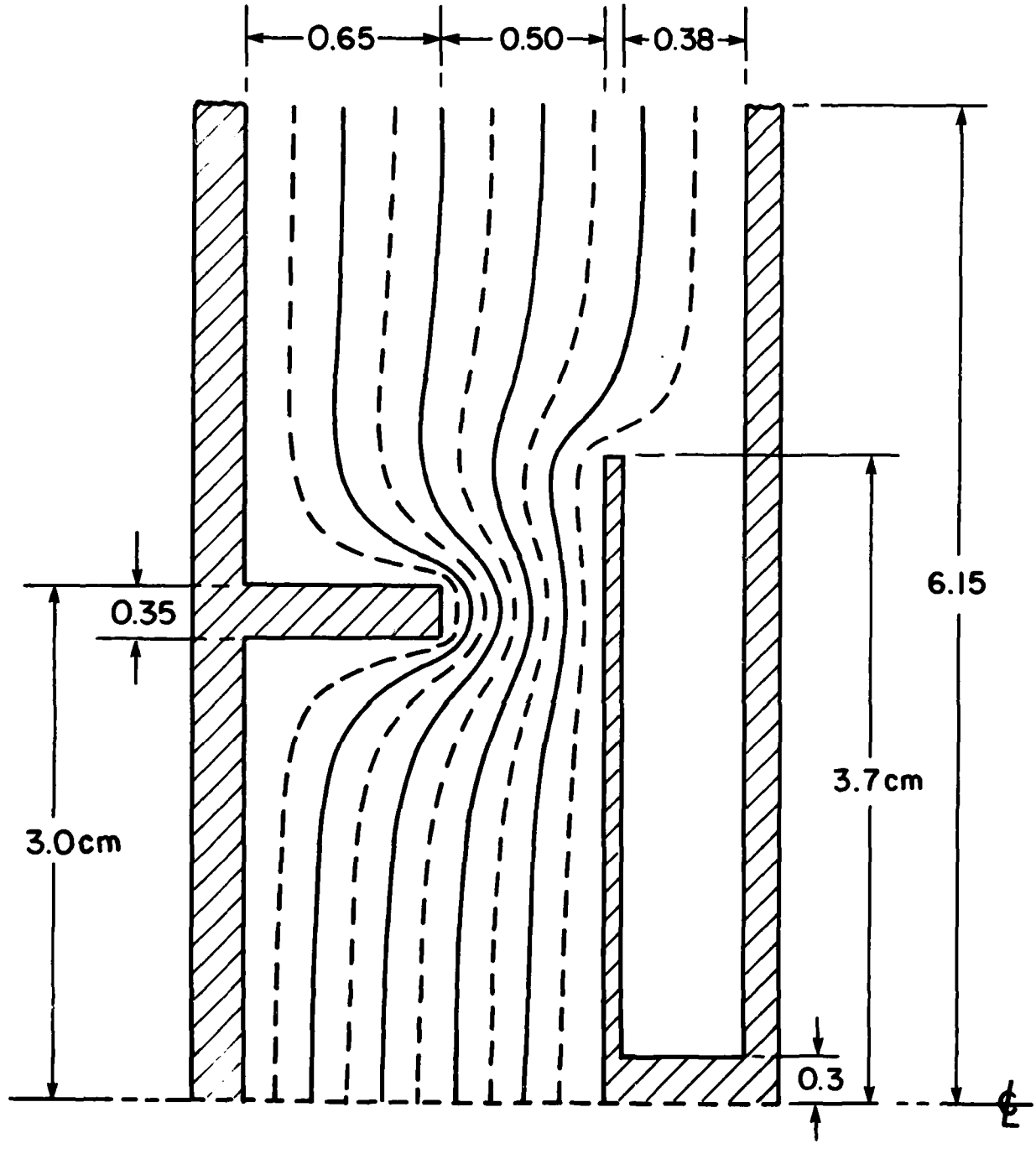

Fig. 3 — Specific geometry of the diode as modeled and its electrostatic equipotential contours with no space charge present

corresponding to an arbitrary $R - Z$ planar cross-section passing through the diode's centerline. Complete azimuthal symmetry is assumed. A finite number of macroelectrons and macroprotons having correct, physical charge-to-mass ratios are advanced timestep-by-timestep across the mesh in a relativistically covariant manner. A self-consistent, steady-state solution is sought both for field structures as well as for particle flows. No time-dependent phenomena are actually treated.

The physical volume simulated by the DIODE2D code extends radially outward from the central axis to a distance of 6.15 cm in the vacuum gap and axially forward from the plane corresponding to the solid cathode face out to the opposing plane surface of the solid anode. Since it presumes azimuthal symmetry, the computer code only deals with a single $R - Z$ planar cross-section extending out from the centerline. This computational region is presented in Figure 4. The grid points are shown as dots and correspond to the centers of their respective rectangular data cells. Counting the monolayer of guard cells which completely surround the numerical region in which "particles" are "allowed," a total of $(NZ + 2) \times (NR + 2) = 66 \times 125 = 8,250$ data cells are used. The bottom boundary corresponds to the central axis ($R = 0$) of the diode. The right boundary corresponds to the solid anode plane and is maintained at the full anode potential, V. The left boundary is kept at zero voltage since it represents the solid cathode plane. Finally, the upper boundary is simply a source-free, vacuum interface between what may be loosely described as the "diode region" and the pulsed power transmission line. The electrostatic potential is therefore graded linearly from zero to V along that upper boundary. Perfectly conducting cathode and anode surfaces are included in the computational region as shown in Figure 4. Those surfaces are treated numerically via a capacitance matrix technique described elsewhere.[14] On the order of 10^4 macroelectrons and 10^4 macroprotons participate in the simulation at steady state. These macroparticles are emitted at their respective electrodes along the heavy-lined surfaces. Axial currents in the cathode shank and in the anode stalk are treated rigorously as a function of z in order to ensure an accurate distribution of B_θ throughout the diode. The results of these numerical simulations as well as a summary of the conclusions which can be drawn from them are presented in the following two sections.

III. SIMULATION RESULTS

In order to test the theorized effects of selective ion emission suppression on the performance characteristics of the diode of Figure 2, three specific test cases were simulated. In all three cases, the diode voltage was fixed at 1.8 MV in accordance with the capabilities of the Gamble II machine. Cases I and II were both run with an A-K (anode-cathode) gap of 5 mm just as shown in Figure 3. Case I corresponded to a "benchmark" run in which no suppression of ion emission on the anode foil was attempted. Protons were emitted along the anode mesh from cells $(IZ,IR) = (48, 2)$ through $(48, 65)$ just as indicated by the heavy line in Figure 4. In Case II, the imposition of a metal foil annulus over the outer anode face was simulated by shutting off ion emission beyond cell (48, 49). Finally, for Case III, the restricted ion emission was retained while all axial dimensions in the simulation were reduced by a factor of 0.70. This changed the A-K gap to 3.5 mm and reduced the diode impedance back to its value in Case I. The detailed results of these simulations are as follows.

Case I was run 4400 timesteps, Δt, of 1.5×10^{-12} seconds each until an equilibrium state was reached. In order to determine the true steady-state values of the quantities of interest a new statistical technique was applied to the numerical data. Specie current values were tabulated at intervals of $25\Delta t$ over the last 200 steps. These values were then subjected to the same type of least squares error analysis and data reduction methods as is normally reserved for the treatment of experimental observations. The details of this new computational approach are presented in the Appendix. The equilibrium ion and electron currents for this "benchmark" case were 230 ± 6 kA and 147 ± 6 kA respectively. Given the diode voltage of 1.8 MV, this yields an impedance of 4.77 ± 0.11 ohms for the device, well within the desired operating regime of 4-5 Ω. The net ion efficiency, $\eta_i \equiv I_{ion}/I_{diode} = I_{ion}/(I_{ion} + I_{electron})$, is then 0.390 ± 0.016. This is in excellent agreement with the 40% ion efficiency recently reported[15] for a numerical simulation of a 2.0 MV, 4 ohm PRD (pinch-reflex diode) having an R/D of 7.58 compared with an R/D of 6.0 for this run. It differs significantly, however from the 0.24

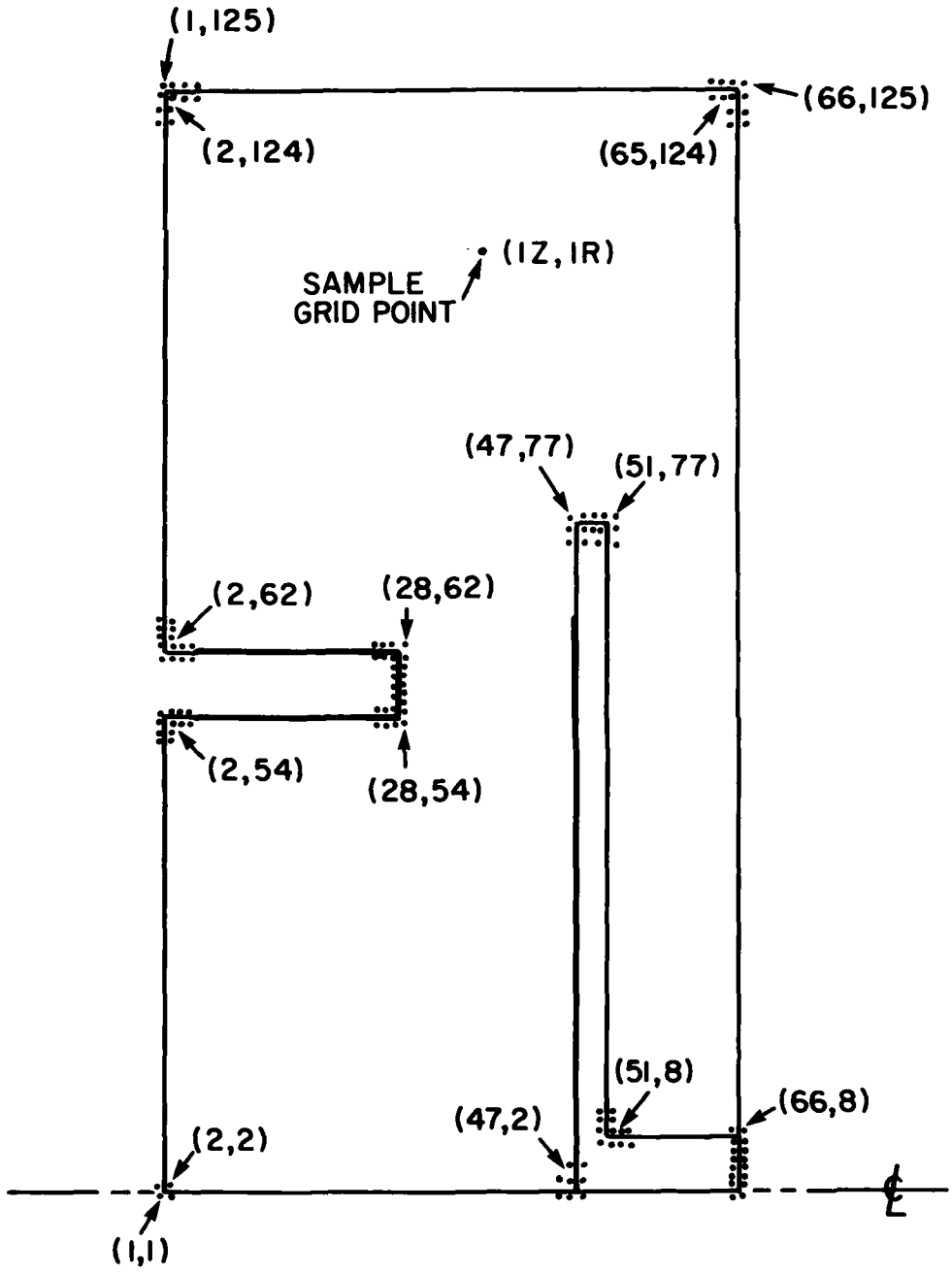

Fig. 4 — Set-up of the numerical simulation region

average ion efficiency reported from a series of Gamble II experimental runs[16] (see Figure 5). At least part of this discrepancy between the numerical and experimental results can be explained by examining Figure 2. The location of the I_{NET} Rogowski coil loop in the experimental set-up shows that it is measuring only that portion of the ion current which hits the "target" inside the cathode shank. Any ions hitting the cathode beyond a radius of 2.25 cm are not counted. To properly compare the numerical results to the experiment, this "effective" ion current must be calculated. Figures 6 and 7 present radial profiles of the emitted and collected ion current densities flowing in the steady state diode. Integrated from these profiles are not only the total ion currents but also the effective currents falling within $R = 2.25$ cm (indicated by the dotted lines). This shows that the empirically measured number should be 119 kA, not 147 kA. This still implies an ion efficiency of 0.316. Although much closer to the experimental data, it is still far from "good" agreement. A more complete explanation for the poor correlation can be found by examining the nature of the electron currents in the diode. That new phenomenon will be discussed after the numerical results for Cases II and III are presented.

Having completed the benchmark run, the next step was to test the effect of restricted ion emission while holding all other diode parameters constant. The maximum radius for ion emission along the anode foil was reduced from $R = 3.2$ cm to $R = 2.4$ cm. Just as for Case I, Case II was run to equilibrium at $t = 4400$ timesteps. At that point, using the same statistical data reduction technique, the currents were found to be $I_e = 186 \pm 3$ kA and $I_i = 83 \pm 2$ kA. These figures imply a diode impedance of 6.69 ± 0.08 ohms and a net ion efficiency of 0.309 ± 0.007. As expected, the impedance has been very significantly raised in spite of the constant A-K gap size, $D = 5$ mm. Once again, to correlate the ion efficiency to the experimental results, the radial profiles of the emitted and collected ion current densities are presented in Figures 8 and 9. An effective I_i of 79 kA is then observed to strike within the "target" radius of 2.25 cm. Interestingly enough, the effective ion efficiency has dropped a mere two percentage points to $(\eta_i)_{eff} = 0.294$ in spite of the 2 ohm impedance rise.

Finally, for Case III the restricted ion emission radius of 2.4 cm was retained while the gap was reduced from 5.0 to 3.5 mm. The observed steady-state diode currents were $I_e = 247 \pm 3$ kA and $I_i = 130 \pm 4$ kA yielding an impedance of 4.77 ± 0.07 ohms and a total ion efficiency of 0.345 ± 0.012. Thus, as expected, the impedance of Case I has been restored in spite of the decreased gap size, D. Although it had been hoped that the ion efficiency would increase, a drop of almost 0.05 was instead recorded. Hopes that a comparison of the effective ion currents would be more optimistic were likewise disappointed. Figures 10 and 11 record the corresponding Case III ion emission and collection profiles. They show that the effective ion current is 119 kA — *exactly* the same as for Case I. Thus the simulations of Case I and Case III share identical impedances *and* identical efficiencies. This is in sharp contrast with the experimental data. The same diode as modeled in Case III fired 28 separate times on Gamble II yielded the modified efficiency data shown in Figure 12 (overlapped with the Case I data). With an average effective ion efficiency of 0.34, it represents a clear departure from the experimental data garnered from the diode without emission restriction and with $D = 5.0$ mm although the average impedances was nearly identical for the two cases. On the other hand, the Case III efficiency figure of 0.34 is in reasonable agreement with the 0.316 measured numerically for both cases.

As previously mentioned, at least a partial explanation for the disagreement between simulation and experiment may rest in the diode's electron flow patterns. The DIODE2D computer code is not electromagnetic; rather, it is electrostatic-magnetostatic. Inductive electric fields are not generated by the particle currents as they should be due to temporal variations in B_θ. This limitation allowed sustained electron currents of huge magnitude to arise between the inside cylindrical surface of the cathode shank and the "target" plane inside the shank. The ability of the ion flow in a diode to draw in electrons to neutralize its space charge is well established.[17] How this neutralizing fill of electron charge maintains itself in the A-K gap is not well understood. At least in this simulation, part of that charge is constantly replenished by the cathode-to-cathode electron currents herein observed. For Case I, this electron current comoving with the ions hitting the "target" region has a magnitude of almost 200 kA.

For Case II it is only about 120 kA. While for Case III it increases slightly again to around 140 kA. It is probable that the inclusion of a physical, inductive *E*-field would greatly reduce the size of those reverse currents. It is questionable if they would be eliminated entirely. If only 20 kA of electron current were left comoving with the ion beam in the detector region for the Case I numerical simulation, the experimentally recorded efficiency of 0.24 would be achieved. It thus seems quite possible that such comoving electrons may be masking some of the true ion current being extracted from the diode in the Case I Gamble II experiment. This theory remains to be tested. Figures 13, 14, and 15 provide plots of sample electron positions (each particle carries the same predetermined amount of charge) for the equilibria of Cases I, II, and III respectively. They show how electron space charge fills the entire interior of the diode. Unfortunately, they do not show explicit flow patterns inside the cathode radius. One thing that does seem clear is the difference in cathode-tip-to-anode-foil electron flow. For Case I, without ion emission suppression, the ion space charge in the gap between the tip and the foil allows electrons to stream almost directly across, thus illuminating the foil face out to about 3 cm with significant negative space charge. Electrons hugging that surface out to large radii encourage enhanced ion emission. On the other hand, Figures 14 and 15 show that elimination of the ion space charge fill near the cathode tip causes much of the electron stream there to pinch radially inward early in its transit of the gap. Thus the mainstream of the electron flow on the average for Cases II and III stays further away from the foil face than in Case I. This reduces expected ion emission and can apparently reduce the ion efficiency benefits of decreasing the gap size, *D*.

IV. CONCLUSIONS

From the results summarized in Table 1, one may conclude that selective ion emission suppression definitely allows the use of smaller *A*-*K* gaps (therefore, higher *R*/*D* ratios) for a fixed diode impedance. This can be beneficial for all light ion beam work in which efficient generator-to-diode power transmission dictates a high diode impedance since a smaller A-K gap means that the ions must spend less time subject to the trajectory-bending effects of the strong electric and magnetic fields found in the diode. The resultant impact on ion beam quality is illustrated in Figures 16, 17, and 18 which plot sample proton equilibrium positions for Cases I, II, and III respectively. The ions are emitted only at data cell centers along the anode face. Thus they are initially spaced out evenly in coaxial, laminar streams. The relative smoothness of each stream may be followed across the gap by tracing from point to point. Significantly less erratic stream behavior is observed in Figure 18 (Case III) with its 3.5 mm gap than for either of Cases I and II in Figures 16 and 17. Although this confirms at least one positive effect of partial ion emission suppression, the simulations did not show any decoupling of the effective ion production efficiency from the diode impedance as was found in the corresponding Gamble II experiments. Although the simulation results are clouded by unrealistically large electron currents comoving with the ion beam, the physical existence of electron currents even an order-of-magnitude smaller than those numerically observed would be sufficient to explain the discrepancy between experiment and simulation.

Two distinct elements of follow-on research should be undertaken. First of all, the simulations described herein should be repeated using a fully electromagnetic computer code. The PREMAS computer code (the successor of DIODE2D at NRL) is currently being upgraded to include time dependent electric and magnetic field solving algorithms. It can be applied to this problem as soon as that coding and debugging is complete. Secondly, an experimental diagnostic technique to separate out the pure ion beam current from any comoving electron component should be designed. The Gamble II runs could then be repeated with such a new diagnostic in place.

ACKNOWLEDGMENTS

The authors are indebted to S. J. Stephanakis for his scientific collaboration, technical advice, and infinite patience over the course of this research and in the preparation of this report.

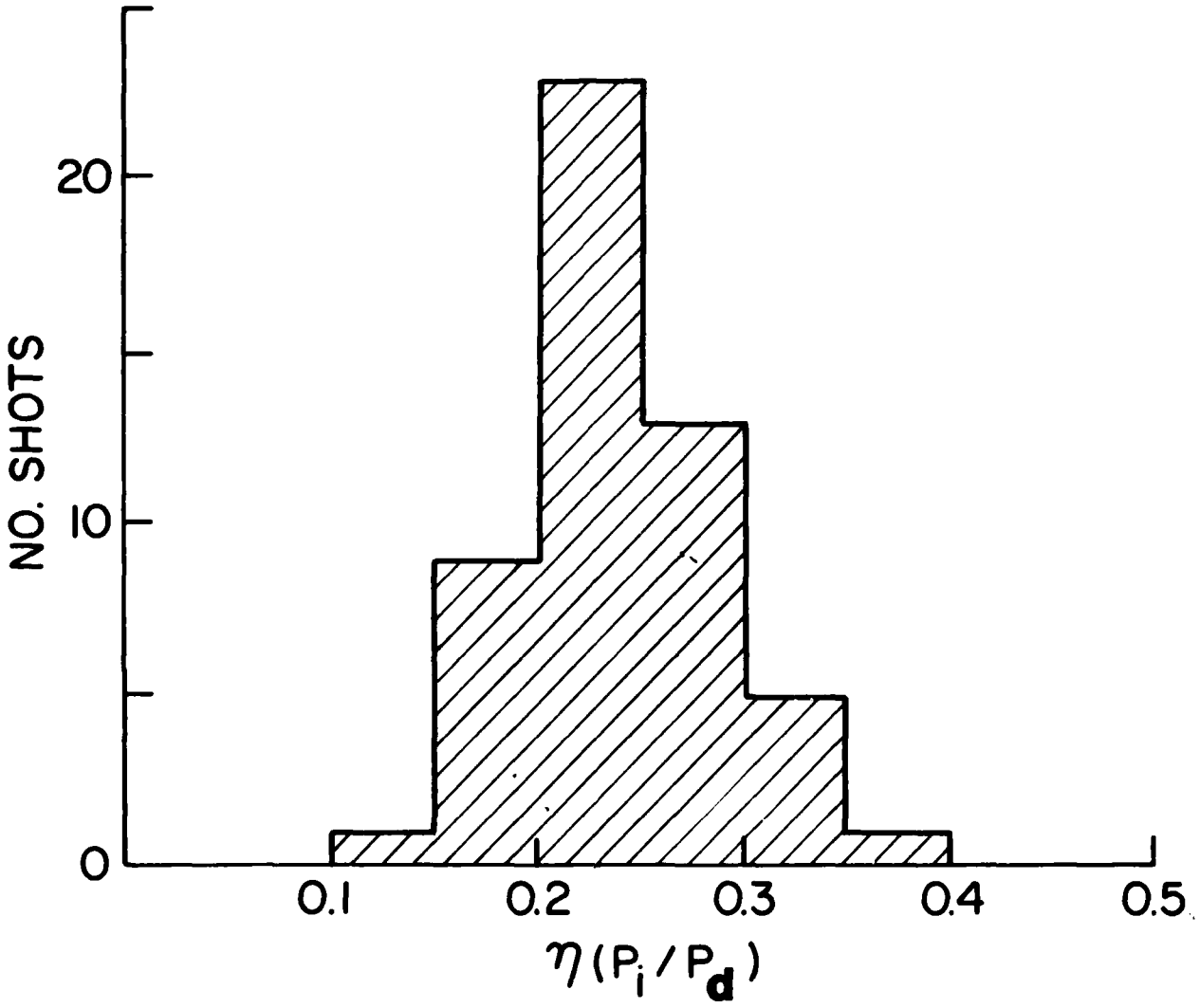

Fig. 5 — Statistical distribution of η_i for the 4Ω Gamble I diode with no ion emission suppression (courtesy of S. J. Stephanakis)

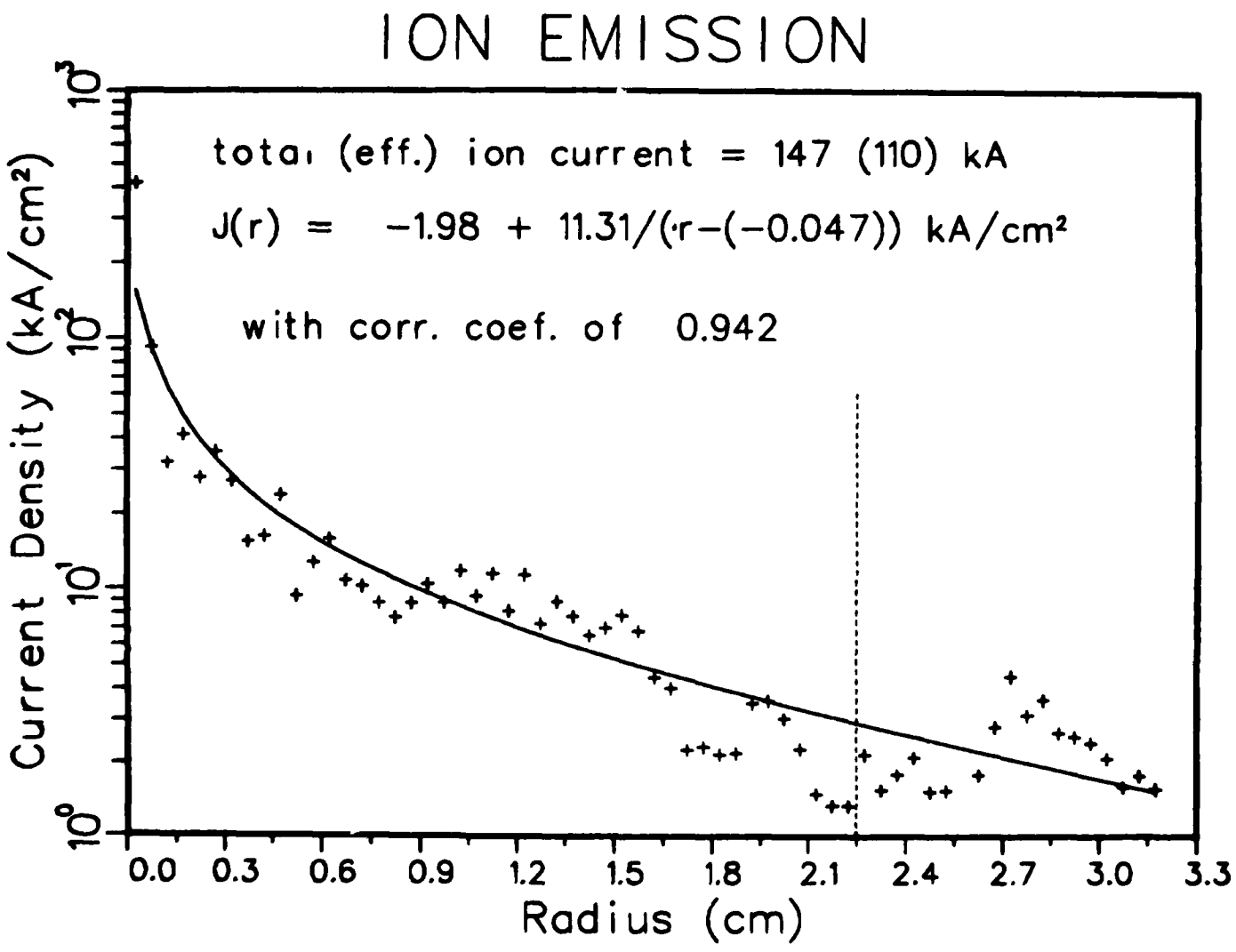

Fig. 6 — Radial profile of emitted ion current density for Case I

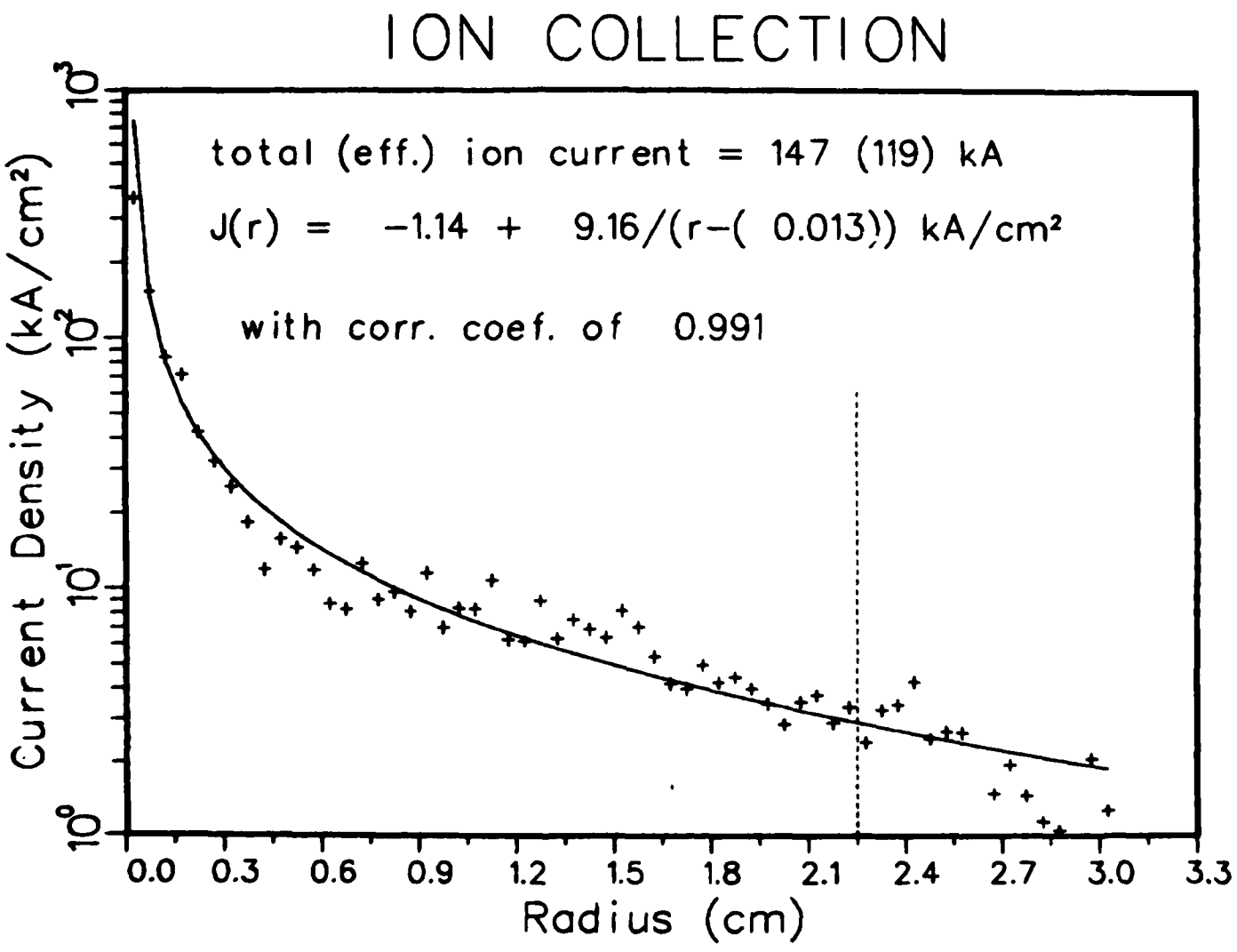

Fig. 7 — radial profile of collected ion current density for Case I

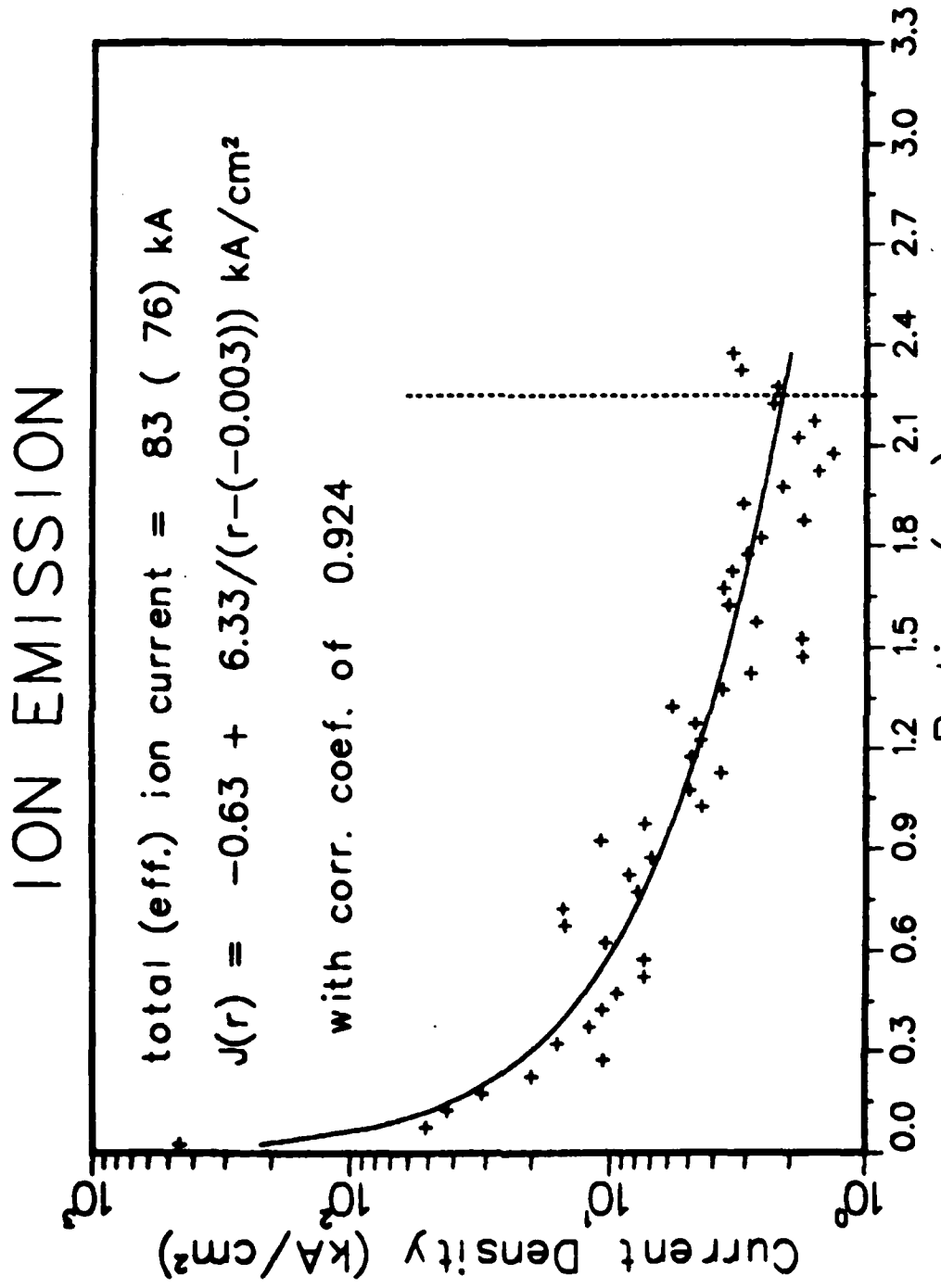

Fig. 8 — Radial profile of emitted ion current density for Case II

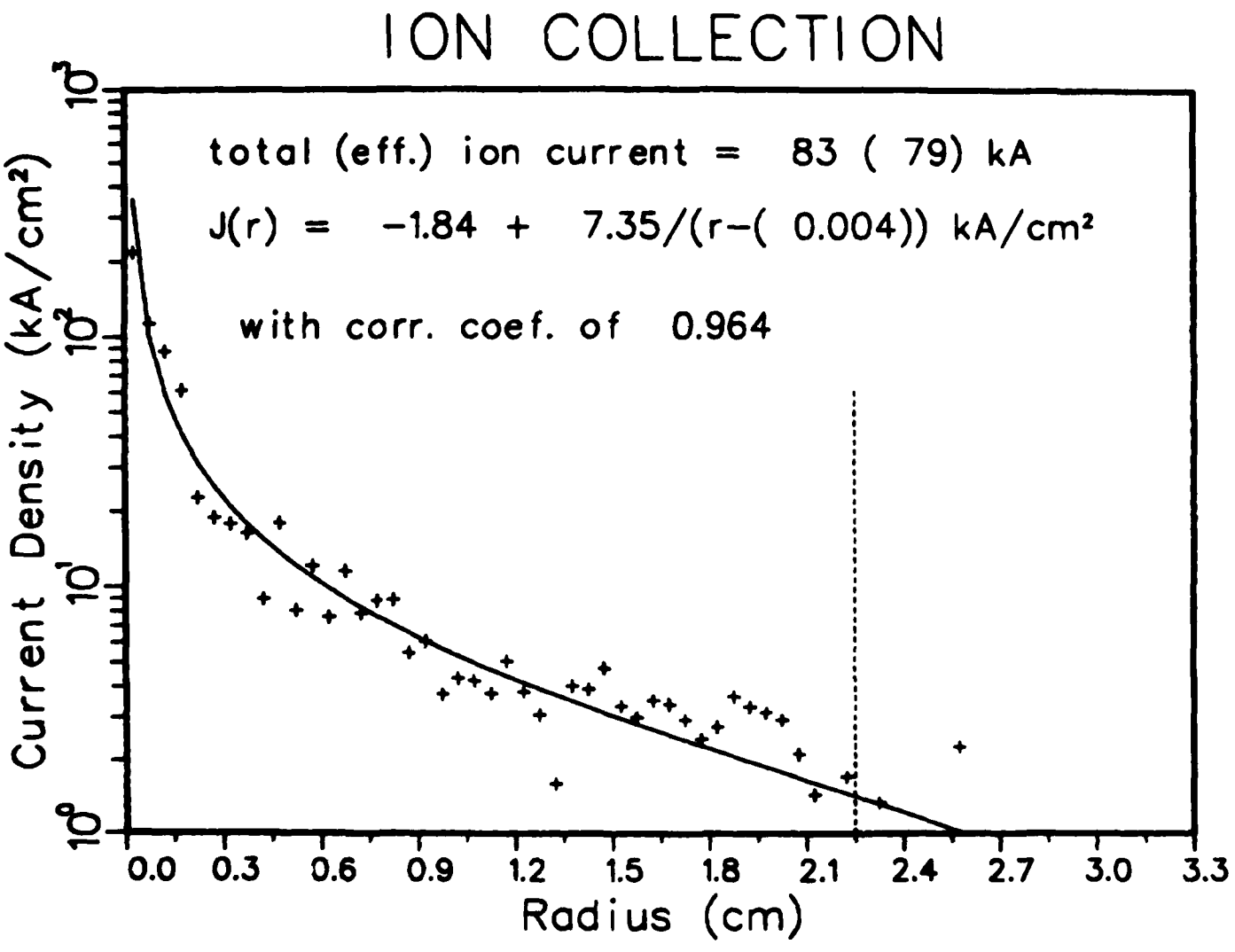

Fig. 9 — Radial profile of collected ion current density for Case II

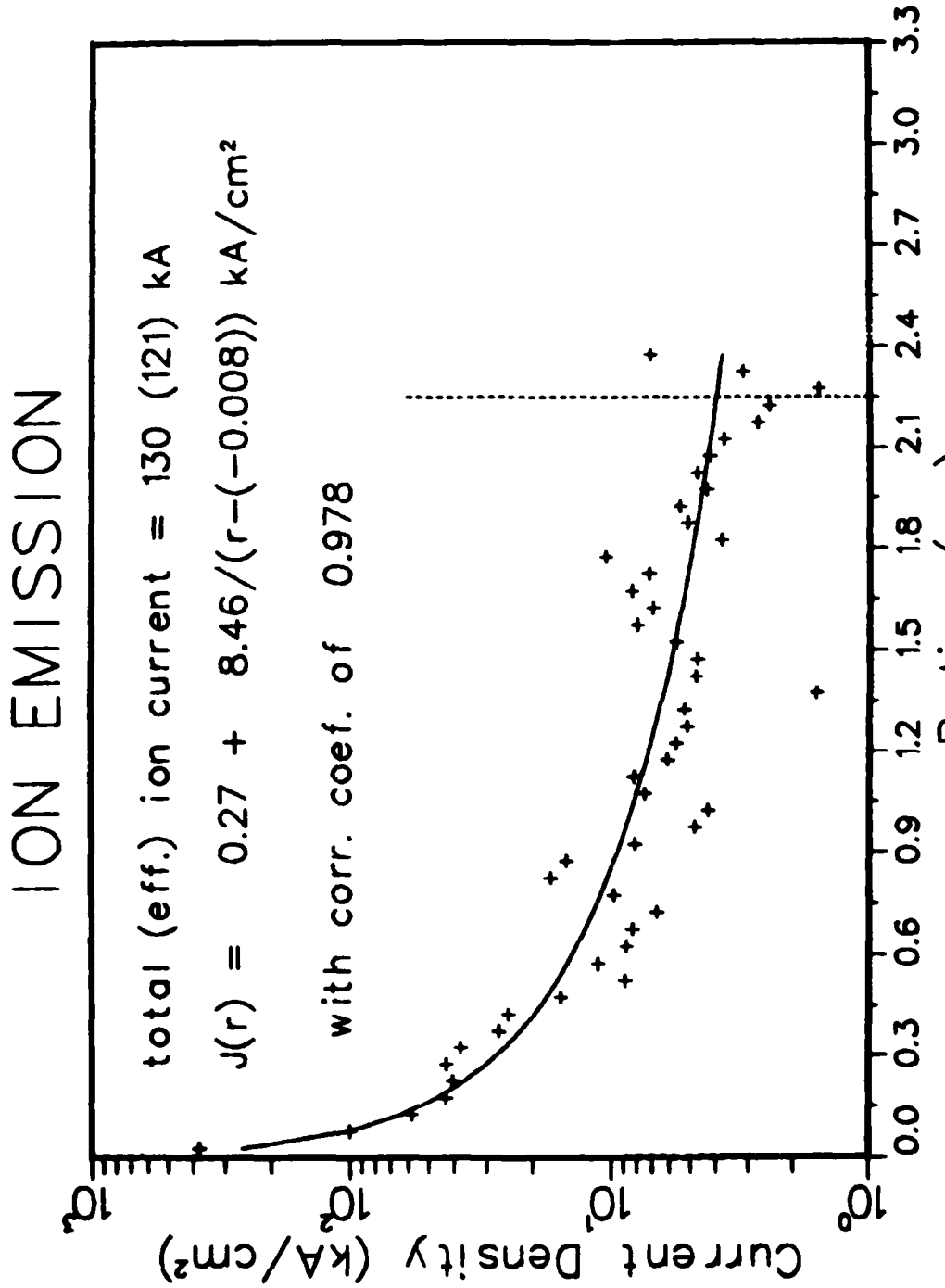

Fig. 10 — Radial profile of emitted ion current density for Case III

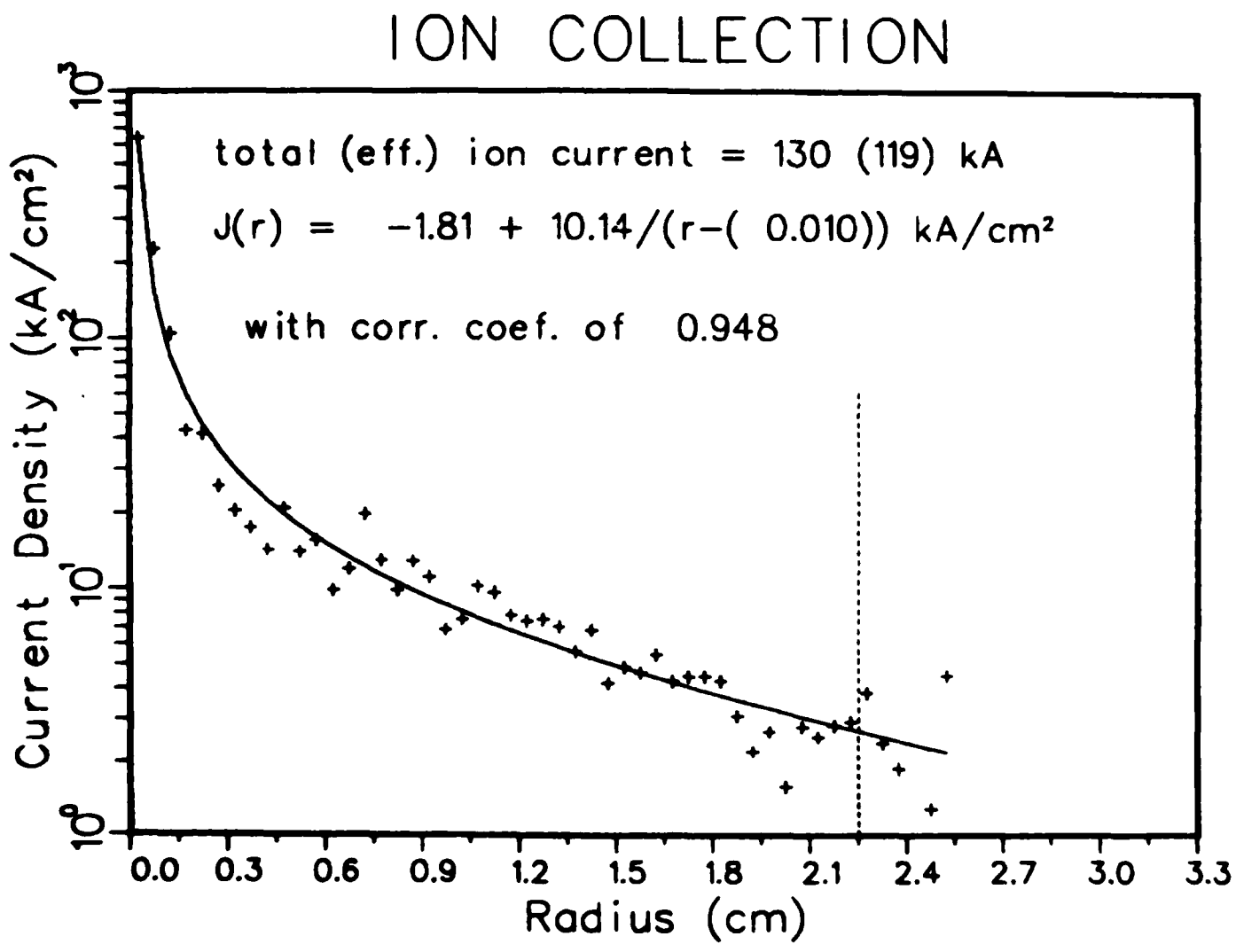

Fig. 11 – Radial profile of collected ion current density for Case III

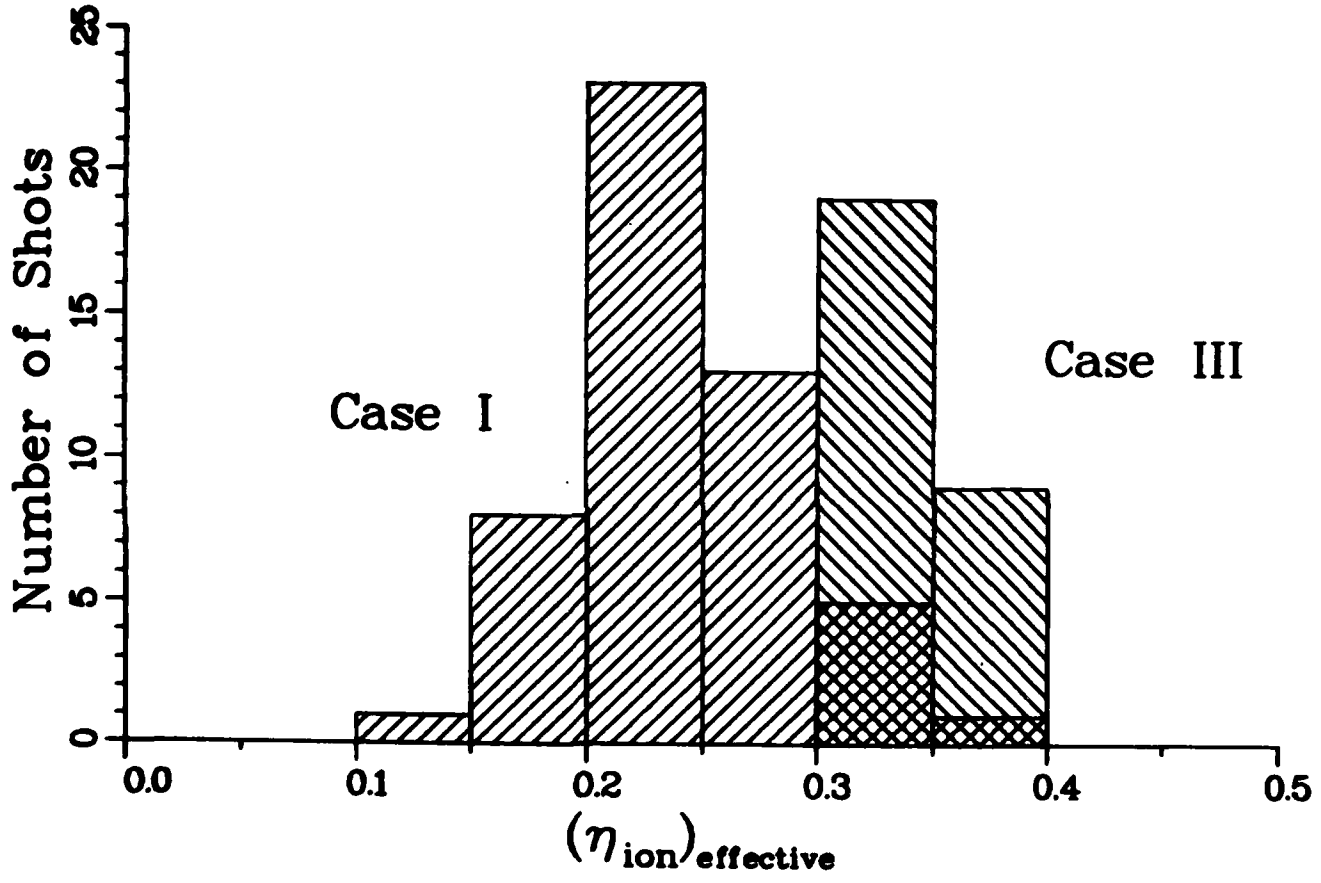

Fig. 12 — Comparison of η_i data collected on Gamble II for 4 Ω diodes with (right) and without (left) selective ion emission suppression

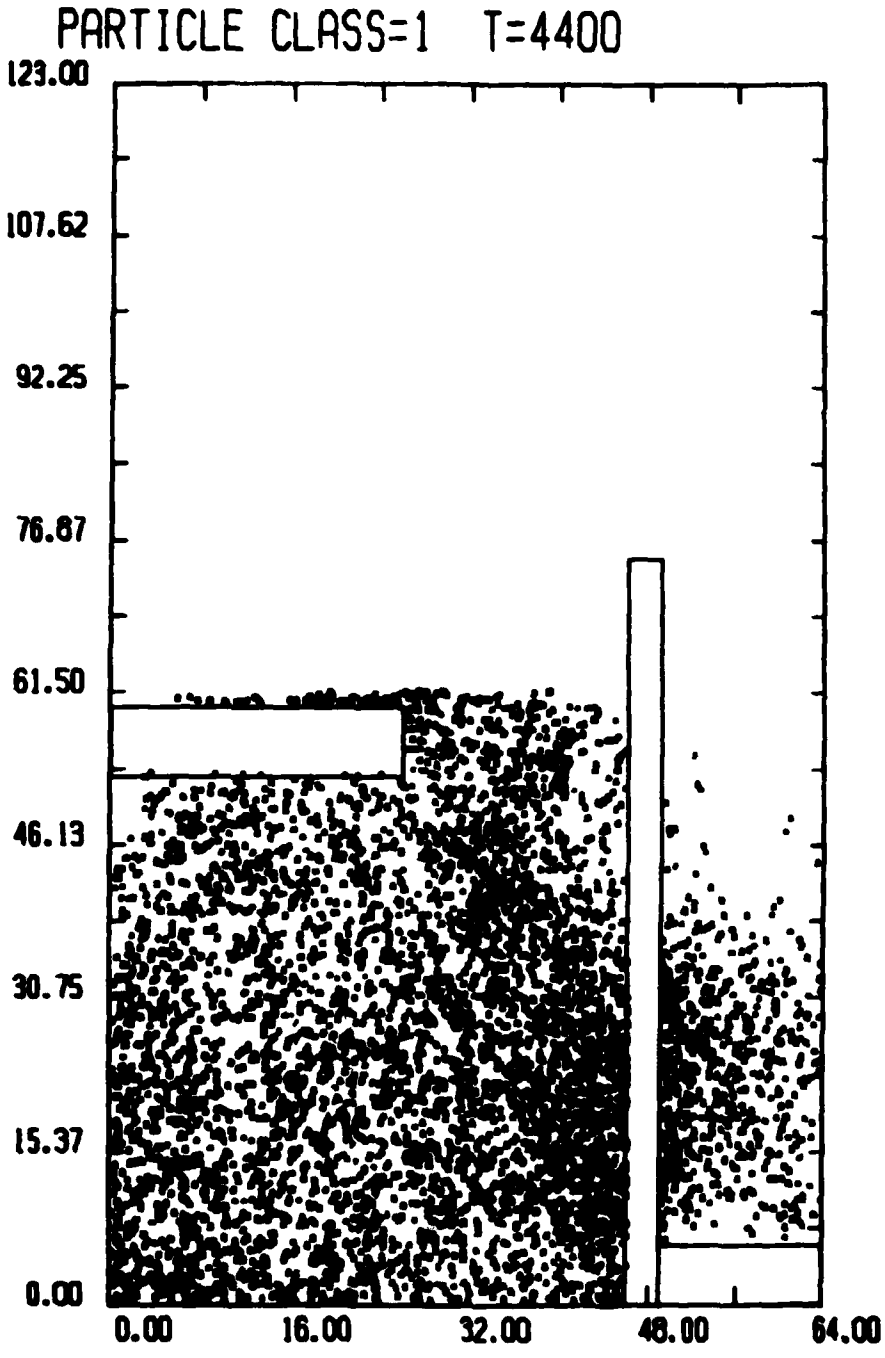

Fig. 13 — Sample steady-state electron plot for Case 1

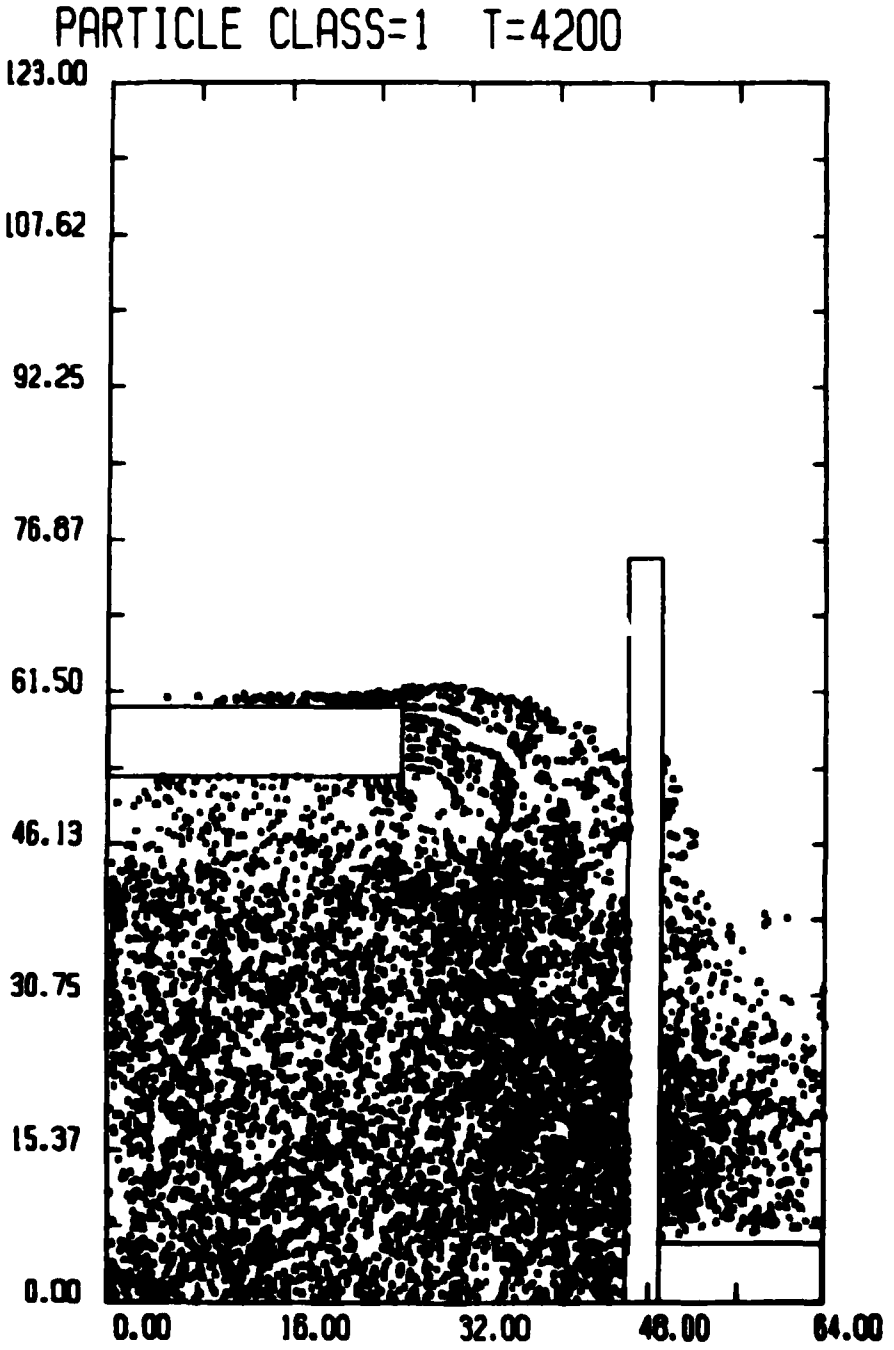

Fig. 14 — Sample steady-state electron plot for Case II

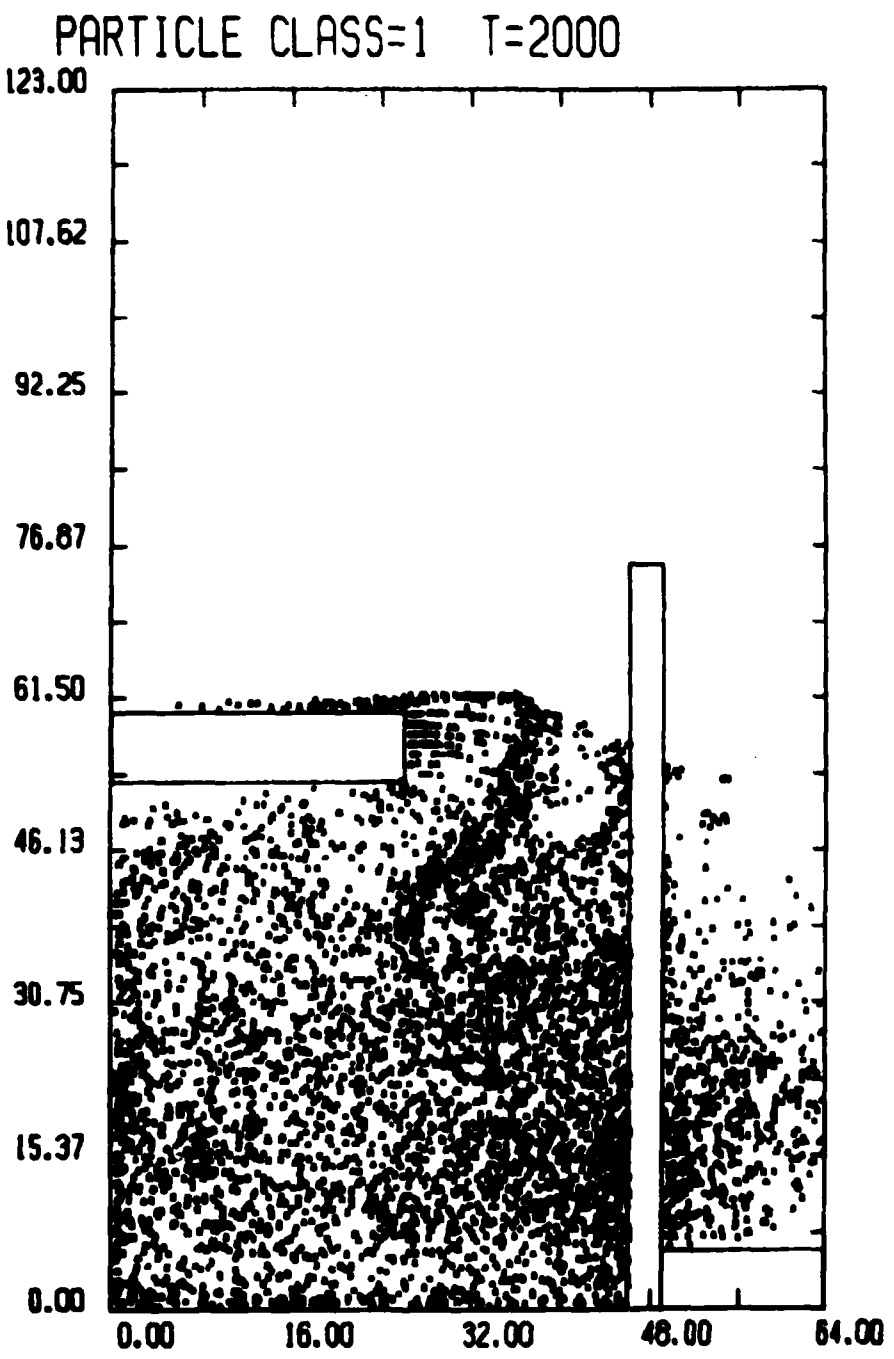

Fig. 15 — Sample steady-state electron plot for Case III

Table 1 — Summary of Computational Results

(ALL AT 1.8 MV)	D = 5.0 MM		D = 3.5 MM
	FULL EMIT CASE I	PART EMIT CASE II	PART EMIT CASE III
$I_{electron}$ (kA)	230 ± 6	186 ± 3	247 ± 3
I_{ion} (kA)	147 ± 6	83 ± 2	130 ± 4
I_{diode} (kA)	377 ± 8	269 ± 3	377 ± 5
$(\eta_{ion})_{net}$	0.39 ± 0.02	0.31 ± 0.01	0.35 ± 0.01
$(I_{ion})_{effective}$	119	79	119
$(\eta_{ion})_{effective}$	0.32	0.29	0.32
Z_{diode} (OHMS)	4.77 ± 0.11	6.69 ± 0.08	4.77 ± 0.07

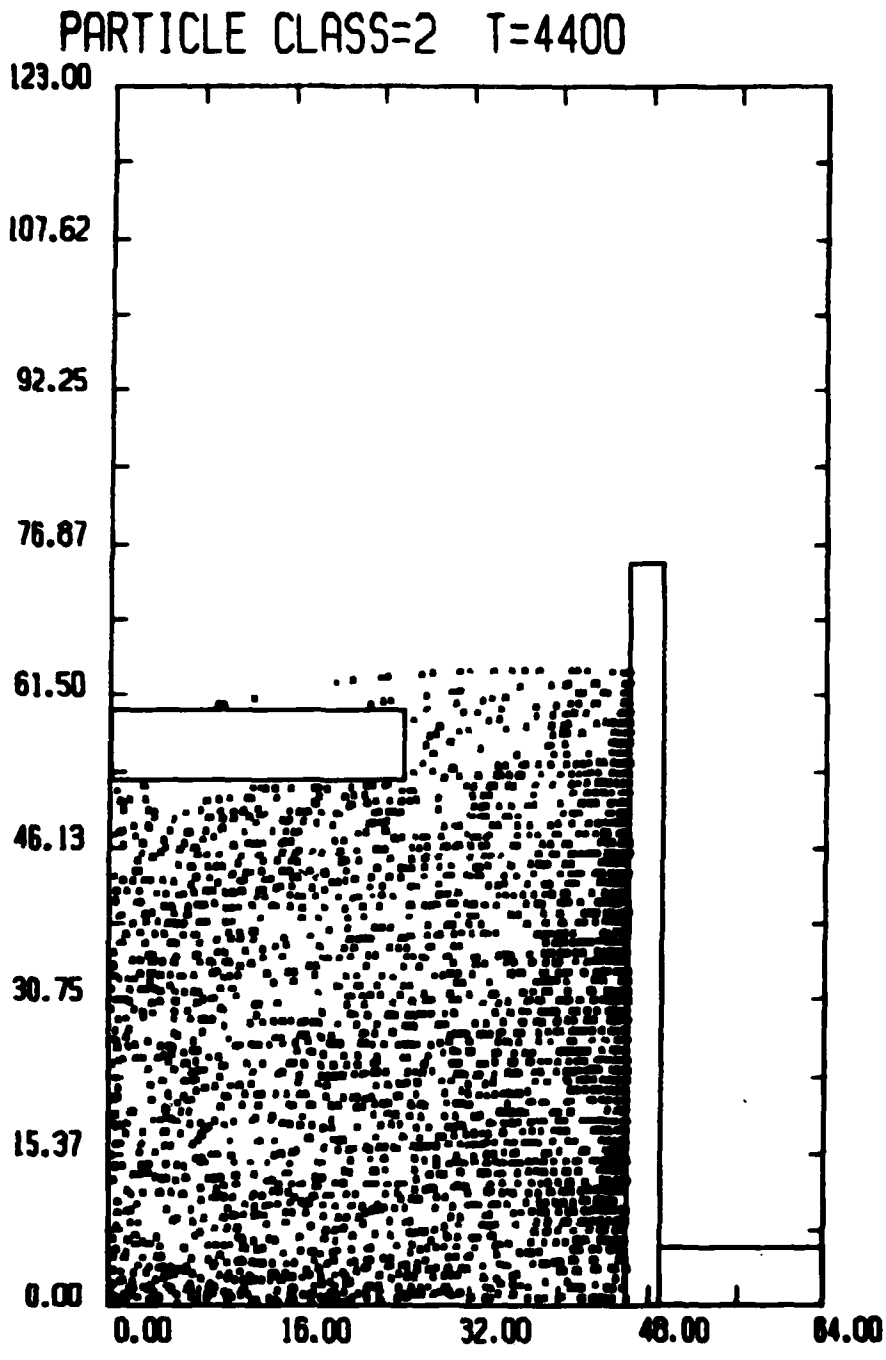

Fig. 16 — Sample steady-state ion plot for Case 1

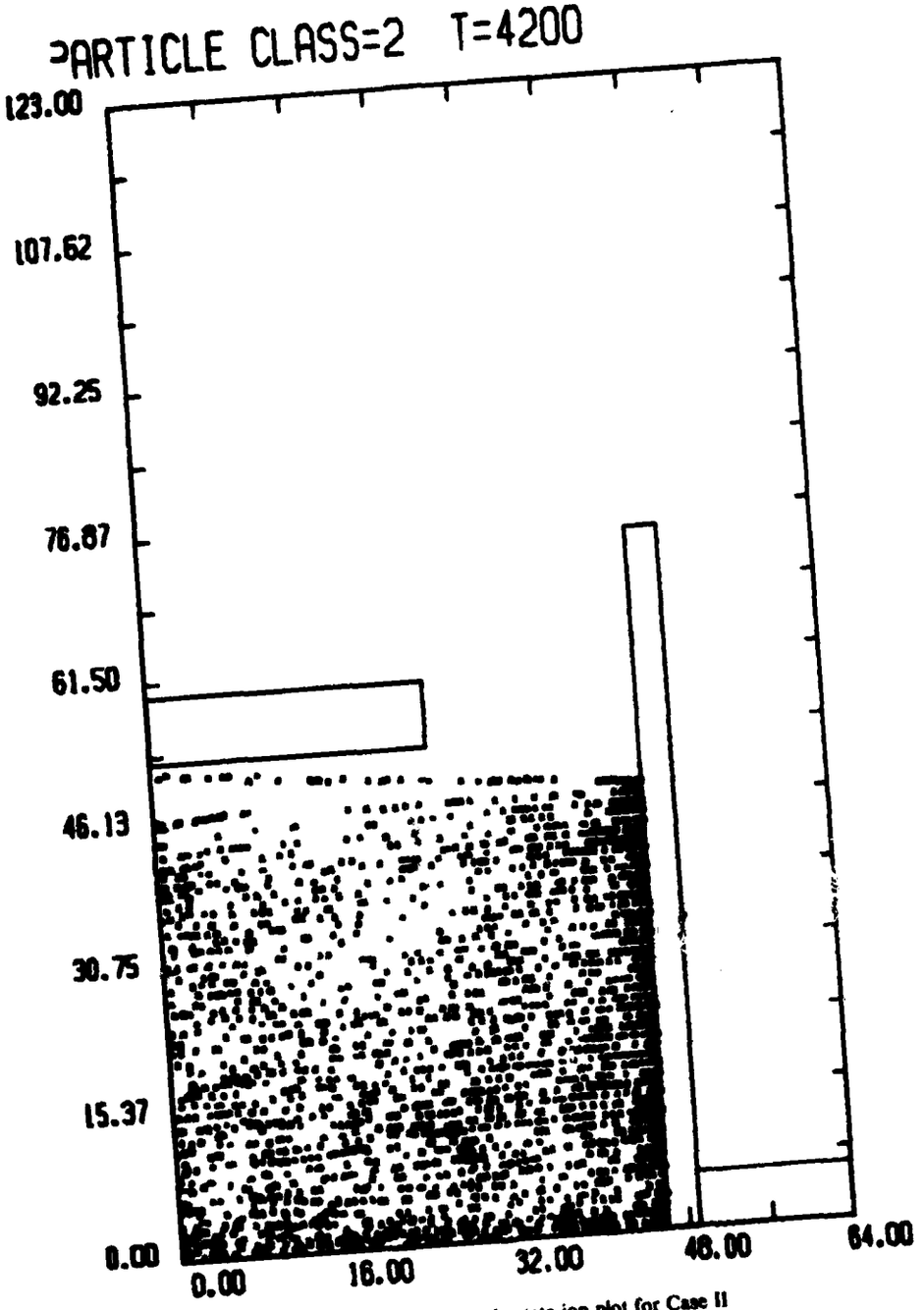

Fig. 17 — Sample steady-state ion plot for Case II

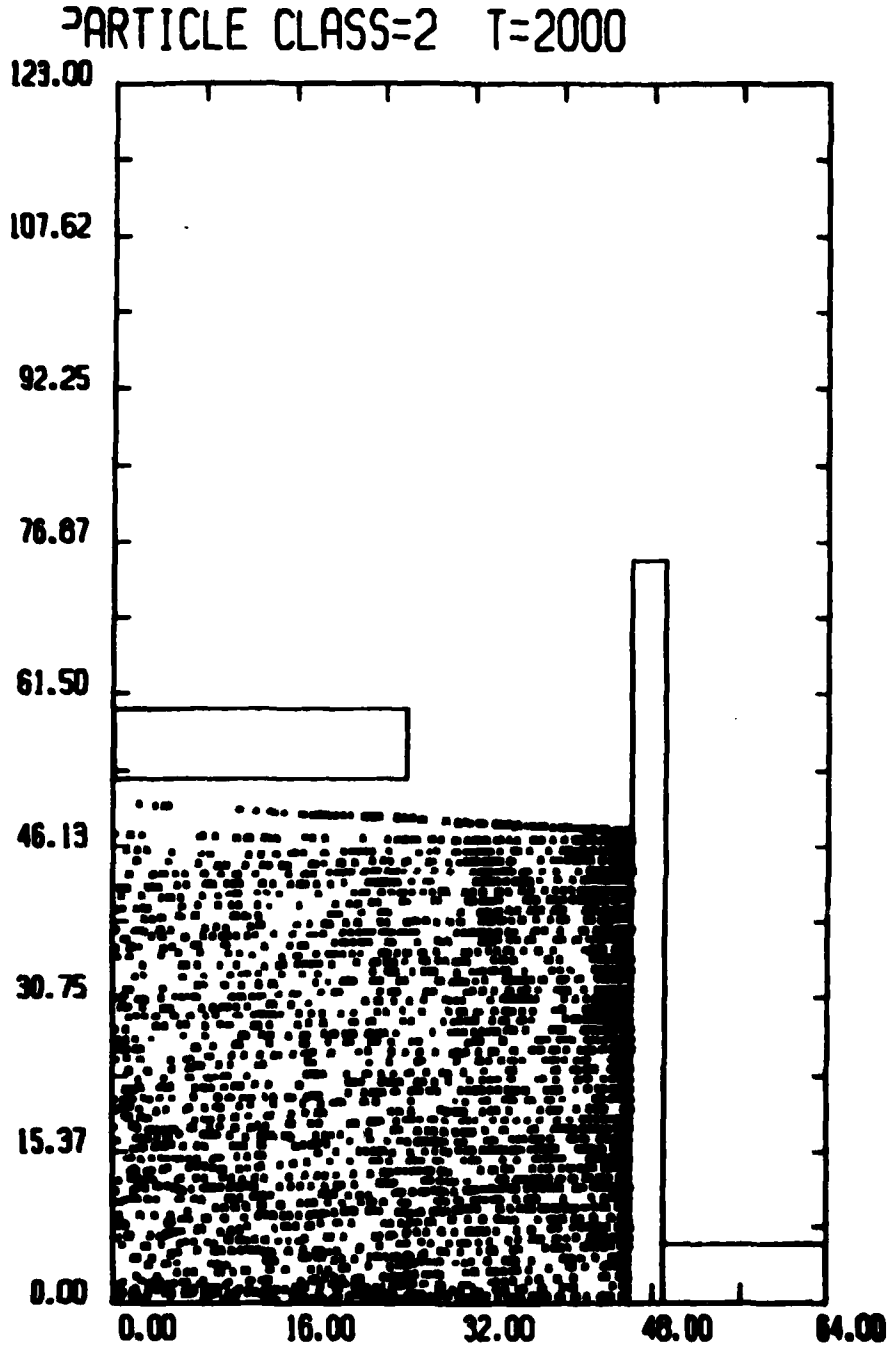

Fig. 18 — Sample steady-state ion plot for Case III

To illustrate the data reduction procedure, the ion current of Case II in this report will be analyzed. The last eight collected ion current values (25 Δt apart) were found to be 83, 81, 87, 84, 82, 78, 93, and 80 kA respectively. This yields a mean value, $<I_{i\text{coll}}>$, of 83.5 kA. To determine the random sampling error associated with that value, the mean value of the square, $<I^2_{i\text{coll}}>$, is found to be 6991.5 kA^2 from which the variance,

$$\sigma_{i\text{coll}} = \sqrt{<I^2_{i\text{coll}}> - <I_{i\text{coll}}>^2} \tag{A.1}$$

is computed to be 4.387 kA. The standard deviation of the mean of the given eight values is then simply

$$(\sigma_{i\text{coll}})_m = \frac{1}{\sqrt{8}}\,\sigma_{i\text{coll}} = 1.55 \text{ kA}. \tag{A.2}$$

Thus, on the basis of the computer-supplied data, the collected ion current for Case II can be written as $(I_i)_{\text{coll}} = 83.5 \pm 1.6$ kA. In exactly the same manner, the last eight emitted ion current values of 97, 99, 112, 73, 48, 85, 77, and 76 kA reduce to a steady-state prediction of $<I_{i_{\text{emit}}}> = 83.4 \pm 6.5$ kA. The much larger standard deviation stems directly from the higher residuals of each data point with respect to their mean value. To arrive at a specific prediction for the net equilibrium ion current flowing through the diode, the weighted average is taken of the emitted and collected ion currents using the method of least squares with

$$I = \frac{<I_{\text{emit}}>/(\sigma_{\text{emit}})^2_m + <I_{\text{coll}}>/(\sigma_{\text{coll}})^2_m}{1/(\sigma_{\text{emit}})^2_m + 1/(\sigma_{\text{coll}})^2_m} \tag{A.3}$$

and

$$\frac{1}{\sigma^2_m} = \frac{1}{(\sigma_{\text{emit}})^2_m} + \frac{1}{(\sigma_{\text{coll}})^2_m}. \tag{A.4}$$

Applying these formulae lead to the result quoted in the text of this report, $I_{\text{ion}} = 83 \pm 2$ kA.

An identical analysis is then applied to find the electron current and its error brackets. The net diode current is then simply

$$I_{\text{diode}} = I_{\text{ion}} + I_{\text{electron}} \tag{A.5}$$

with

$$(\sigma_{\text{diode}})^2_m = (\sigma_{\text{ion}})^2_m + (\sigma_{\text{electron}})^2_m. \tag{A.6}$$

From this quantity flows the expressions for the diode impedance, z, and ion production efficiency η_i. For the impedance, one may write $z = V/I_{\text{diode}}$ where V is the constant diode voltage. The standard deviation from the mean of this quantity is then given by

$$(\sigma_z)^2_m = \left[\frac{V}{I^2_{\text{diode}}}\right]^2 (\sigma_{\text{diode}})^2_m. \tag{A.7}$$

Similarly, the ion production efficiency, $\eta_i = I_{\text{ion}}/I_{\text{diode}}$, has a standard deviation found from the expression,

$$(\sigma_{\eta_i})^2_m = \left[\frac{I_{\text{ion}}}{I^2_{\text{diode}}}\right]^2 (\sigma_{\text{diode}})^2_m + \left[\frac{(\sigma_{\text{ion}})_m}{I_{\text{diode}}}\right]^2. \tag{A.8}$$

The above equations summarize the error analysis which flows naturally from the reduction of raw, numerical data. It provides a simple framework for the statistically valid presentation of steady-state computer simulation code results for diode physics research.

Appendix

STATISTICAL TREATMENT OF COMPUTATIONAL DATA

Whenever numerical predictions extracted from computer simulations are cited in the literature they are almost always presented without any indication of the error brackets associated with those predictions. Conventional error analysis such as that performed routinely for experimental data is traditionally ignored by many computational physicists. When one analyzes a given physical system using a computer simulation code, the numerical data distilled from the code is just as prone to systematic and random sampling errors as that gleaned from a physical experiment. Programming flaws in the code as well as physical flaws and resolution limits in the simulation model will introduce systematic errors into the resulting data. Similarly, when dealing with a computer code which attempts to find the steady-state operating conditions of a given system, periodic sampling of the parameters of interest as they relax into their equilibrium values will give rise to random errors around the "true" values. Both types of errors can be quantified in order to allow an outside observer to know how much weight he should give to the computational results.

The identification and minimization of gross systematic errors contained in the algorithms of a given computer code is normally accomplished once and for all before a given code is accepted for use in production simulation runs. Careful debugging using a variety of standard test cases can eliminate numerical deviations from true physics that go beyond established assumptions for the systems to be modeled. In addition to computer programming bugs, there are also the finite resolution limitations inherent in any digitized model. Some of these, such as standard numerical "round-off" errors can be made insignificant through clever coding of the numerical algorithms. Other sources of error such as the finite number of spatial data points and the finite number of particles used, give rise to actual "minimum errors" which can have significant sizes compared with the values of interest and which can only be lowered by changing the numerical parameters or by rewriting sections of the computer code itself. Any potential user of the simulation results must rely upon the professional abilities of the individual computational physicist regarding the removal of all "bugs" from his code. On the other hand, the user must be aware that there *will* definitely be some systematic errors due to numerical discreteness.

The treatment of random sampling errors is less a question of computational talents then of scientific rigor. Observationally obtained data is inherently bracketed by error bars. Only a finite number of samples of data can be obtained from a given system. Like its physical counterpart, a numerical system cannot be truly static. It will oscillate around an equilibrium state and it is at various points on these "ripples" that the diagnostic data is output from the program. Therefore, random sampling errors must occur and they can be quantified using conventional, statistical treatments. The data reduced for presentation in this report may be used to illustrate the procedure. The major macroscopic quantity monitored in these simulations is the net current flowing through the diode. This current is made up of an electron and an ion component. For each specie component, the emitted current and the collected current are measured separately. Therefore, there are four "subcurrents" that are directly monitored and must be analyzed separately. In a given DIODE2D simulation run, the subcurrents and net charges in the system are tallied every 25 timesteps. After some specific "risetime" is passed, these quantities begin to oscillate around certain plateau values. Such behavior signals the system's arrival at an equilibrium state. At that point, the last eight subcurrent data values spanning the last 200 timesteps are reduced to arrive at approximate steady state predictions for the diode being modeled.

For this specific problem of light ion diode error analysis, another element of statistical analysis, namely — curve fitting, was employed. Its purpose was to obtain the best possible analytic approximation for the radial profile of the ion current density exiting the diode. Such an explicit representation for $J(r)$ is useful particularly for theoreticians attempting to model the transport of the emerging ion beam away from the diode through a predetermined transport channel.[18,19] Previous simulations have observed an approximate inverse proportionality of the current density to the radius.[20] A functional form of

$$J(r) = J_0 + a(r - r_0)^{-1} \tag{A.9}$$

is therefore chosen as the starting point. The raw data of averaged ion emission and collection at each mesh point in the r-dimension along the anode and cathode respectively are first plotted as single points (see Figures 6-11). Then a curve of form (A.9) is fitted to it. In order to obtain that curve, the method of least squares[21] is employed. The three unknowns in the equation are then given by

$$J_0 = D^{-1} \begin{vmatrix} \Sigma\ J_i r_i^2 & \Sigma\ r_i & \Sigma\ J_i r_i \\ \Sigma\ J_i r_i & N & \Sigma\ J_i \\ \Sigma\ J_i^2 r_i & \Sigma\ J_i & \Sigma\ J_i^2 \end{vmatrix} \tag{A.10}$$

$$r_0 = D^{-1} \begin{vmatrix} \Sigma\ r_i^2 & \Sigma\ r_i & \Sigma\ J_i r_i^2 \\ \Sigma\ r_i & N & \Sigma\ J_i r_i \\ \Sigma\ J_i r_i & \Sigma\ J_i & \Sigma\ J_i^2 r_i \end{vmatrix}$$

$$a = J_0 r_0 + D^{-1} \begin{vmatrix} \Sigma\ r_i^2 & \Sigma\ J_i r_i^2 & \Sigma\ J_i r_i \\ \Sigma\ r_i & \Sigma\ J_i r_i & \Sigma\ J_i \\ \Sigma\ J_i r_i & \Sigma\ J_i r_i & \Sigma\ J_i^2 \end{vmatrix}$$

where

$$D = \begin{vmatrix} \Sigma\ r_i^2 & \Sigma\ r_i & \Sigma\ J_i r_i \\ \Sigma\ r_i & N & \Sigma\ J_i \\ \Sigma\ J_i r_i & \Sigma\ J_i & \Sigma\ J_i^2 \end{vmatrix}$$

and where the summations are from $i = 1$ to $i = N$ (N being the number of radial data points), r_i is the radius of the "i"th point, and J_i is the observed $J(r_i)$. The "goodness" of the fit of the data to the curve thus generated can be gauged by comparing the root mean square deviation of the data points from the curve to the root mean square deviation of those same points from their average value $\langle J \rangle = N^{-1} \Sigma\ J_i$. The resultant "correlation coefficient" may then be expressed as[22]

$$\sqrt{1 - \frac{\Sigma\ (J_i - J_0 - a(r_i - r_0)^{-1})^2}{\Sigma\ (J_i - \langle J \rangle)^2}}. \tag{A.11}$$

It should be noted that in practice some care must be exercised in the application of (A.11) to the problem in question. Near $r = 0$, the values of J become quite large so that deviations from the smoothed fit tend to be exaggerated. To avoid that distortion, the data at $r = r_1$ is ignored in the calculation of (A.11) as presented in Figures 6 through 11.

REFERENCES

1. G. Cooperstein, R.J. Barker, et al., in Proceedings of the United States-Japan Symposium on the Theory and Application of Multiply Ionized Plasmas Produced by Laser and Particle Beams, Japan (1982).

2. D.J. Johnson, G.W. Kuswa, A.V. Farnsworth, Jr., and J.P. Quintenz, et al., Phys. Rev. Lett. **42**, 610 (1979).

3. G. Cooperstein, S.A. Goldstein, and D. Mosher, et al., in Proceedings of the 3rd Internationl Topical Conference on High Power Electron and Ion Beam Research and Technology, Novosibirsk, USSR (1979).

4. D.J. Johnson, Bull. Am. Phys. Soc. **24**, 925 (1979).

5. S.J. Stephanakis, J.R. Boller, G. Cooperstein, S.A. Goldstein, D.D. Hinshelwood, D. Mosher, W.F. Oliphant, F. Sandel, and F.C. Young, Bull. Am. Phys. Soc. **23**, 907 (1978).

6. D.G. Colombant, S.A. Goldstein, and D. Mosher, Phys. Rev. Lett. **45**, 1253 (1980).

7. R.A. Meger, F.C. Young, A. T. Drobot, G. Cooperstein, S.A. Goldstein, and D. Mosher, NRL Memo. Report 4477 (1981).

8. D.J. Johnson, S.A. Goldstein, R. Lee, and W.F. Oliphant, J. Appl. Phys. **49**, 4634 (1978).

9. S.A. Goldstein and R. Lee, Phys. Rev. Lett. **35**, 1079 (1975).

10. A. E. Blaugrund, G. Cooperstein, and S.A. Goldstein, Phys. Fluids **20**, 1185 (1977).

11. S.J. Stephanakis, private communication.

12. S.J. Stephanakis, R.J. Barker, S.A. Goldstein, and W.F. Oliphant, IEEE Conf. on Plasma Science **1C9**, Santa Fe, New Mexico (1981).

13. R.J. Barker, A.T. Drobot, R. Lee, and S.A. Goldstein, Proc. 9th Conf. on the Numerical Simulation of Plasmas, Evanston, Ill. (1980).

14. R.J. Barker, Banach Center Publications **3**, 255, Warsaw, Poland (1975).

15. R.J. Barker and S.A. Goldstein, NRL Memo. Report 4773 (1982).

16. S.J. Stephanakis, S.A. Goldstein, D. Mosher, and W.F. Oliphant, Bull. Am. Phys. Soc. **25**, 900 (1980).

17. R.J. Barker, S.A. Goldstein, and A.T. Drobot, NRL Memo. Report 4642 (1981).

18. D.G. Colombant, D. Mosher, and S.A. Goldstein, NRL Memo. Report 4252 (1980)

19. P.F. Ottinger, S.A. Goldstein, and D. Mosher, NRL Memo. Report 4548 (1981).

20. R.A. Meger, F.C. Young, et al., NRL Memo. Report 4477 (1981).

21. H.D. Young, *Statistical Treatment of Experimental Data,* McGraw-Hill, New York (1962).

22. E.L. Crow, F.A. Davis, and M.W. Maxfield, *Statistics Manual,* Dover, New York (1960).

KMS Fusion, Inc.
3941 Research Park Drive
P.O. Box 1567
Ann Arbor, MI 48106
Attn: Alexander A. Glass 1 copy

Lawrence Berkeley Laboratory
Berkeley, CA 94720
Attn: D. Keefe 1 copy

Lawrence Livermore National Laboratory
P.O. Box 808
Livermore, CA 94550
Attn:
Tech. Info. Dept. L-3 1 copy
D.J. Meeker 1 copy
R.E. Batzel/J. Kahn,L-1 1 copy
J.L. Emmett, L-488 1 copy
J.F. Holzrichter, L-481 1 copy
W.F. Krupke, L-488 1 copy
J.H. Nuckolls, L-477 1 copy

Los Alamos National Laboratory
P.O. Box 1663
Los Alamos, NM 87545
Attn: M. Gillispie/Theo.Div. 1 copy
S.D. Rockwood,ICF Prog. Mgr.
DAD/IF M/S 527 6 copies

Massachusetts Institute of Technology
Cambridge, MA 02139
Attn: R.C. Davidson 1 copy
G. Bekefi 1 copy

Maxwell Laboratories, Inc.
9244 Balboa Avenue
San Diego, CA 92123
Attn: J.Pearlman 1 copy

Mission Research Corporation
1400 San Mateo Blvd. SE
Albuquerque, NM 87108
Attn: B.B. Godfrey 1 copy

National Science Foundation
Mail Stop 19
Washington, DC 20550
Attn: D. Berley 1 copy

Naval Research Laboratory
Addressee: Attn: Name/Code
Code 2628 -TID Distribution 25 copies
Code 4000 - T. Coffey 1 copy
Code 4040 - J. Boris 1 copy

Naval Research Laboratory
Addressee: Attn: Name/Code
Code 4700 - S.L. Ossakow 26 copies
Code 4704 - C. Kapetanakos 1 copy
Code 4720 - J. Davis 1 copy
Code 4730 - S. Bodner 1 copy
Code 4740 - V. Granatstein 1 copy
Code 4760 - B. Robson 1 copy
Code 4770 - I.M. Vitkovitsky 10 copies
Code 4771 - F. C. Young 1 copy
Code 4773 - G. Cooperstein 10 copies
Code 4773 - S.J. Stephanakis 1 copy
Code 4790 - D. Colombant 1 copy
Code 4790 - I. Haber 1 copy
Code 4790 - M. Lampe 1 copy
Code 6682 - D. Nagel 1 copy

Office of Naval Research
London Branch Office
Box 39
FPO New York, NY 09510
Attn: Dr. David Mosher 1 copy

Physics International Co.
2700 Merced Street
San Leandro, CA 94577
Attn: A.J. Toepfer 1 copy

Pulse Sciences, Inc.
1615 Broadway, Suite 610
Oakland, CA 94612
Attn: S. Putnam 1 copy

R&D Associates
Suite 500
1401 Wilson Blvd.
Arlington, VA 22209
Attn: P.J. Turchi 1 copy

R&D Associates
P.O. Box 9695
Marina Del Rey, CA 90291
Attn: C. MacDonald 1 copy

Sandia National Laboratories
P.O. Box 5800
Albuquerque, NM 87185
Attn: G.W. Kuswa / 4240 6 copies
J.P. Vandevender/4254 1 copy

Spire Corporation
P.O. Box D
Bedford, MA 01730
Attn: R.G. Little 1 copy

JULY 1982

DISTRIBUTION FOR JOINT DNA AND DOE SPONSORED WORK

Director
Defense Nuclear Agency
Washington, DC 20305
Attn: TISI Archieves — 1 copy
TITL Tech. LIbrary — 3 copy
J. Z. Farber (RAEV) — 1 copy
H. Soo (RAEV) — 1 copy
M. Fellows (RAEV) — 1 copy

U.S. Department of Energy
Division of Inertial Fusion
Washington, DC 20545
Attn: T.F. Godlove — 1 copy
S.L. Kahalas — 1 copy
R.L. Schriever — 1 copy

U.S. Department of Energy
Office of Classification
Washington, DC 20545
Attn: Robert T. Duff — 1 copy

U.S. Department of Energy
Nevada Operations Office
Post Office Box 14100
Las Vegas, NV 89114
Attn: Rex Purcell — 2 copies

U.S. Department of Energy
P.O. Box 62
Oak Ridge, TN 37830 — 1 copy

Air Force Office of Scientific Research
Physics Directorate
Bolling AFB, DC 20332
Attn: A. K. Hyder — 1 copy
M. A. Stroscio — 1 copy

Air Force Weapons Laboratory, AFSC
Kirtland AFB, NM 87117
Attn: NTYP (W. L. Baker) — 1 copy

Atomic Weapons Research Establishment
Building H36
Aldermaston, Reading RG 7 4PR
United Kingdom
Attn: J.C. Martin — 1 copy

Boeing Company, The
P.O. Box 3707
Seattle, WA 98124
Attn: Aerospace Library — 1 copy

Brookhaven National Laboratory
Upton, NY 11973
Attn: A.F. Maschke — 1 copy

BMO/EN
Norton AFB, CA
Attn: ENSN — 1 copy

Commander
Harry Diamond Laboratory
2800 Powder Mill Rd.
Adelphi, MD 20783
(CNWDI-INNER ENVELOPE: ATTN: DELHD-RBH)
Attn: DELHD-NP — 1 copy
DELHD-RCC -J.A. Rosando — 1 copy
DRXDO-RBH - K. Kerris — 1 copy
DRXDO-TI - Tech Lib. — 1 copy

Cornell University
Ithaca, NY 14850
Attn: D.A. Hammer — 1 copy
R.N. Sudan — 1 copy

Defense Advanced Research Project Agency
1400 Wilson Blvd.
Arlington, VA 22209
Attn: R. L. Gullickson — 1 copy

Defense Technical Information Center
Cameron Station
5010 Duke Street
Alexandria, VA 22314
Attn: T.C. — 2 copies

JAYCOR, Inc.
205 S. Whiting Street
Alexandria, VA 22304
Attn: J. Guillory — 1 copy

Kaman Tempo
816 State Street (P.O. Drawer QQ)
Santa Barbara, CA 93102
Attn: DASIAC — 1 copy